

Contents lists available at ScienceDirect

Petroleum Science

journal homepage: www.keaipublishing.com/en/journals/petroleum-science



Original Paper

Organic petrographic investigation for artificially matured marine shale: Insights from anhydrous pyrolysis of Upper Ordovician shale from the Baltic Basin, Lithuania



Ye Wang ^{a, *}, Zhong-Liang Ma ^{b, c}, Nan-Sheng Qiu ^{d, **}, Bao-Jian Shen ^b, Xiao-Min Xie ^e, Tenger Borjigin ^f, Lun-Ju Zheng ^{b, c}, Zhao-Xi Zuo ^{b, c}, An-Yang Pan ^{b, c}

- ^a School of Earth Science and Resources, Key Laboratory of Western Mineral Resources and Geological Engineering of Ministry of Education, Chang'an University, Xi'an, 710054, Shaanxi, China
- ^b State Key Laboratory of Shale Oil and Gas Enrichment Mechanisms and Effective Development, SINOPEC, Beijing, 102206, China
- ^c Wuxi Research Institute of Petroleum Geology, Sinopec Petroleum Exploration and Production Research Institute, Wuxi, 214126, Jiangsu, China
- d State Key Laboratory of Petroleum Resources and Engineering, China University of Petroleum (Beijing), China, 102249, China
- ^e Key Laboratory of Oil and Gas Resources and Exploration Technology, Ministry of Education, College of Resources and Environment, Yangtze University, Wuhan, 430100, Hubei, China
- f Oil and Gas Survey Center, China Geological Survey, Beijing, 100083, China

ARTICLE INFO

Article history: Received 29 October 2024 Received in revised form 27 January 2025 Accepted 21 March 2025 Available online 24 March 2025

Edited by Jie Hao

Keywords:
Thermal maturity
Vitrinite-like particle
Zooclast
Anhydrous pyrolysis
Equivalent vitrinite reflectance
Organic pore

ABSTRACT

The absence of humic vitrinite complicates the determination of thermal maturity in pre-Devonian sediments. Lower Paleozoic shales contain structured zooclasts, solid bitumen, and vitrinite-like materials, and their reflectances have been found to be valid maturity proxies. Yet there remains much controversy as to the degree of evolution of reflectances. The current work aims to investigate the reflectance of dispersed organic matter (DOM), as well as their transformation degree and organic pore development. To this end, this study evaluated an Upper Ordovician zooclasts-bearing shale and a Middle Jurassic coal sample via anhydrous-pyrolysis to compare differences in the maturation pathways between marine-derived DOM and terrigenous vitrinite. These two original samples were cut into small blocks and placed in an identical vacuum stainless vessel simultaneously. The pyrolysis was carried out at isothermal temperatures ranging from 250 to 550 °C for 48 h. The morphologic and reflectance changes of DOM in pyrolysis residues were studied and compared with previous pyrolysis results.

Adopting the combined use of optical reflectance and scanning electron microscope (SEM) techniques, the study shows that DOM in the shale components consists of solid bitumen (SB), bituminite, chitinozoans, a few graptolites, vitrinite-like particles (VLP), alginate and liptodetrinite. The reflectance sequence, from high to low, is zooclasts, VLP and SB. Their reflectances gradually increases as the pyrolysis temperature rises, although the rate of growth is slower than that of co-heating coal vitrinite. Notably, zooclasts yield significantly higher reflectance values than those of VLP and SB at each pyrolysis temperature. However, the VLP undergoes two distinct phases in reflectance development, despite gradual morphology changes similar to vitrinite. Based on evidence of the optical texture and organic pore evolution, we argue that a fair amount of VLP in studied Upper Ordovician shale does not consist of graptolite-type fragments. Consequently, the VLPRo serves as a reliable indicator for assessing organic matter maturity in Ordovician shales with a reflectance value of less than 2.0%. This investigation enhances scholarly understandings of marine-derived DOM evolution issues, providing clearer correlations among reflectances of different DOM and reducing uncertainties in thermal maturity determination.

© 2025 The Authors. Publishing services by Elsevier B.V. on behalf of KeAi Communications Co. Ltd. This is an open access article under the CC BY-NC-ND license (http://creativecommons.org/licenses/by-nc-nd/

4.0/).

E-mail addresses: wangy@chd.edu.cn (Y. Wang), qiunsh@cup.edu.cn (N.-S. Qiu).

^{*} Corresponding author.

^{**} Corresponding author.

1. Introduction

Increasing interest in shale oil and gas exploration and development has raised some questions regarding thermal maturity assessment in Lower Paleozoic organic-rich shales (Hackley and Cardott, 2016; Mastalerz et al., 2018; Hackley et al., 2018). Vitrinite reflectance (VR₀) is considered as the most robust maturity indicator for determination of thermal maturity for hydrocarbon exploration and basin research (Hackley et al., 2015; Hackley and Cardott, 2016; Schito et al., 2017, 2019). However, thermal maturity determination for Lower Paleozoic shales is challenging and complex because the lack of vitrinite renders its difficulty (Mastalerz et al., 2018; Wang et al., 2020; Luo et al., 2025). Previous works have shown that marine derived organic zooclasts such as graptolite and chitinozoan occurring in Lower Paleozoic sedimentary series could be used for maturity determinations, since their optical properties change systematically with sediment maturation (Goodarzi et al., 1985; Goodarzi and Norford, 1987, 1989; Bustin et al., 1989; Bertrand et al., 2003; Bertrand and Malo, 2012; Lavoie et al., 2016; Sorci et al., 2020). Bertrand and Yvon Héroux (1987) proposed preliminary correlations between zooclast reflectances and those of vitrinite, which Bertrand (1990) further refined. Graptolite reflectance was widely used to assess maturity for Lower Paleozoic shales in different regions around the world (Cole, 1994; Gentzis et al., 1996; Luo et al., 2020 and references therein). The optimal approach to assess maturity of Lower Paleozoic marine shales is to integrate optical, geochemical, and spectroscopic thermal proxies (Hartkopf-Fröder et al., 2015; Petersen et al., 2013; Synnott et al., 2018; Schito et al., 2019; Spina et al., 2021; Buratti et al., 2024). Recent studies have shown that graptolite random reflectance (GR₀) is more reliable thermal maturation proxy than the reflectance of solid bitumen in vitrinite-lacking pre-Devonian sediments, especially the Wufeng-Longmaxi shales with extremely high maturity (Luo et al., 2018; Wang et al., 2019). Furthermore, graptolite reflectance and its application was reviewed by Luo et al. (2020). Yet limited scholarly attention has been paid to chitinozoan reflectance (CR_o) due to its low abundance (Tricker et al., 1992; Obermajer et al., 1996; Haeri-Ardakani et al., 2015; Cichon-Pupienis et al., 2021). Furthermore, the distinction of zooclasts for Lower Paleozoic sediments in the Baltic Basin remain unclear in earlier studies (Zdanavičiūtė and Lazauskienė, 2009; Caricchi et al., 2016; Coltoi et al., 2016; Sorci et al., 2020).

In addition, there is also a type of dispersed organic matter (DOM) in Paleozoic source rocks known as vitrinite-like materials. They were referred to as vitrinite-like maceral (VLM) or vitrinitelike particle (VLP) as in early studies (Buchardt and Lewan, 1990; Zhong and Qin, 1995; Wang et al., 1996; Xiao et al., 2000; Schmidt et al., 2015; Reyes et al., 2018; Luo et al., 2021). Buchardt and Lewan (1990) recorded one type of discrete solitary OM particles, revealed their similarity with vitrinite, and then proposed the concept of vitrinite-like maceral (VLM). Besides, they discovered a negative relationship between its reflectance and kerogen H/C ratios. The hydrous pyrolysis experiments show that the reflectance of VLM is similar to that of suppressed vitrinite. The VLM is easily confused with broken zooclast fragments dispersed in sediments (Petersen et al., 2013). Following that, various studies explored its reflectance evolution laws and the responses to thermal stress, and compared it to vitrinite reflectance characteristics based on artificial thermal matured source rocks via a hydrous or anhydrous pyrolysis system (Zhong and Qin, 1995; Wang et al., 1996; Xiao et al., 2000; Schmidt et al., 2015; Reyes et al., 2018; Luo et al., 2021). So far, however, its identification and origin remain controversial. Therefore, VLM is not recognized as a maceral by the International

Committee for Coal and Organic Petrology (ICCP)/The Society for Organic Petrology (TSOP) and is excluded from the DOM classification (Gonçalves et al., 2024). Given the above controversy, the study uses VLM and VLP interchangeably to refer to the same material.

Regarding the origin of VLM/VLP, it is generally acknowledge that: (1) VLM in Alum shale is assumed to be an original and primary maceral derived from the gelation of polysaccharides (Buchardt and Lewan, 1990). (2) Because of their comparable optical properties and shape, the VLP are assumed to represent graptolite fragments (Petersen et al., 2013; Teng et al., 2022). (3) VLP is classified as a kind of solid bitumen that does not exhibit pore-filling characteristics (Schmidt et al., 2019), and is derived from the in-situ residue products of algae degradation in Middle Ordovician oil shale (Kukersite), Estonia (Wang et al., 1996). (4) VLM in Carboniferous marine source rock of southwest Tarim Basin originates from faunal organic matter formed through biochemical degradation rather than solid bitumen, which is not the product of oil cracking (Xiao et al., 1997). (5) Based on comparative analysis via non-hydrous thermal treatment, Luo et al. (2021) infer that VLM is bacterial degradation of lamalginite and/or bituminite in Mesoproterozoic Xiamaling shale from North China, whereas, in Cambrian (Series 3—Furongian) Alum shale, it may be akinete cells. Using closed hydrous pyrolysis, Reyes et al. (2018) assessed the degree of physicochemical alteration of DOM of Upper Ordovician shale from Hudson Bay Basin and analyzed the reflectance correlations among graptolite, chitinozoan, and VLP. Actually, VLP is easily confused with zooclast and solid bitumen due to its distinct shape and similar morphological properties. Without a pore and fracture filling, embayment or matrix form, SB is difficult to be distinguished from VLP (Schmidt et al., 2019). It is referred to as vitrinite-like solid bitumen by Mählmann and Bayon (2016). Further, maceral identification and maturity determination with isolated kerogen polished blocks is more challenging. This is due to the destruction of the original occurring form of organic matter. At the same time, incorrect identification of maceral might lead to a misunderstanding of thermal maturity as well as development of organic pores (Hackley and Cardott, 2016).

Based on the above questions and arguments, it is obvious that samples from a wider range of maturity and various basins worldwide have to be compared and thoroughly examined. Although hydrous pyrolysis provides more accurate simulations of natural hydrocarbon generation, no more than 2% maturity was attained compared to closed anhydrous pyrolysis (Hackley and Lewan, 2018; Cavelan et al., 2019). Because of the limited maturity reached by hydrous pyrolysis, it can be difficult to completely examine the evolutionary behavior of vitrinite-like materials at higher maturity levels, and little work has been done on their optical properties and associated organic pore development combined with SEM petrography. Therefore, knowledge about the thermal evolution behavior and process of vitrinite-like materials is still quite limited. Hence, our investigation intends to examine and compare the marine-derived OM with terrigenous vitrinite at higher level of maturity. Anhydrous co-pyrolysis experiments were performed on both an Upper Ordovician zooclasts-bearing shale and a Middle Jurassic coal sample in this study. Organic petrographic investigation was conducted on the reflectance and morphology evolution of the original samples and residual pyrolysis products by means of combined optical and SEM properties. The aims of the present study were to (1) investigate the transformation degree and organic pore development for marinederived DOM; (2) compare with the existing datasets to explore the possible application of vitrinite-like material as a thermal maturity proxy for Lower Paleozoic organic-rich shales.

2. Samples and experiments

2.1. Samples

The Upper Ordovician zooclasts-bearing marine shale was collected from borehole drilling in the Baltic Basin, Lithuania. The Ordovician succession is mainly characterized by clayey and detrital limestones with fossil remains, marlstone, and mudstone/claystone horizons (Paškevičius, 1997). Lithologically, the black shale contained calcareous lenticular fabrics and bioclasts (Fig. 1). The geological setting of the Baltic Basin and petroleum system have been reported by several publications (Vecoli et al., 2011; Kotarba and Lewan, 2013; Cichon-Pupienis et al., 2021) and hence, will not be reviewed here. Besides, a humic coal of Middle Jurassic Xiahuayuan Formation was collected for comparative purpose from Cuijiazhai coal mine located in Hebei Province, China.

2.2. Experiments

2.2.1. Geochemical analyses

Rock-Eval pyrolysis were conducted by Rock-Eval 6 instrument according to standardized procedures described by Espitalié et al. (1985). Following Carvajal-Ortiz and Gentzis (2015), total organic carbon (TOC, wt%) was determined using a LECO 230 analyzer after the powdered samples were treated with hydrochloric acid to remove carbonate minerals. The results were collected from experimental reports available in Wuxi Research Institute of Petroleum Geology, Sinopec.

2.2.2. Anhydrous pyrolysis

For anhydrous pyrolysis equipment, the investigation was carried out with a WYMN-3 high-temperature and high-pressure thermal simulation instrument (Fig. 2). Closed anhydrous pyrolysis was performed using a closed vacuum stainless steel plug and cap as a reactor without added water. Briefly, an aliquot of shale and coal samples were simultaneously loaded into a pre-cleaned reactor. The reactor was sealed and then put into a pyrolysis autoclave. Prior to pyrolysis, the sealing capacity was examined. Nitrogen gas was injected at a pressure of 4–6 MPa to check the system's airtightness. When no gas leaks occurred, we employed vacuum pump to remove nitrogen gas to maintain a vacuum. 3–5 rounds of filling with and releasing nitrogen were repeated before we emptied the reactor and commenced heating. These samples were isothermally heated for 48 h at temperatures of 250, 300, 350,



Fig. 1. The original sample of the Upper Ordovician shale from the Baltic Basin, Lithuania.

400, 450, 500 and 550 °C, respectively. The autoclave was heated at a rate of 1 °C/min. The 48 h experiment durations did not include the time required for the oven to heat to the experimental temperature and to cool to room temperature. After pyrolysis experiments, the stainless-steel autoclaves were withdrawn from the pyrolysis oven and naturally cooled to the room temperature. The pyrolyzed samples were prepared for organic petrographic analyses and reflectance measurements as described below.

2.2.3. Organic petrography and optical reflectance

The original and pyrolyzed residual shale samples were prepared for organic petrography including visual maceral examination in reflected white and ultra-violet (UV) light sources, and optical reflectance measurements were made on polished resinembedded blocks according to ASTM-D7708 (2015). Organic petrology was carried out on samples cut perpendicular to the bedding plane using polished blocks. For co-matured coal samples, however, they were crushed in a jaw crusher to ~1 mm top size. The hardened molded blocks were then grounded and polished according to Wang et al. (2023).

In final preparation for microscopy using a Leica DM4500P microscope equipped with a MPS 200 microphotometer for reflectance measurements. Reflected light microscopy revealed that solid bitumen was excessively fine-grained. Their reflectance measurements were conducted using a OLYMPUS BX53M microscope with the Diskus Fossil system software. The equipment was calibrated by Yttriumc-Aluminiumc-Garnet ($R_{\rm o}\%=0.90$), Gadolinium-Gallium-Garnet ($R_{\rm o}\%=1.72$), and Cubic-zirconia ($R_{\rm o}\%=3.17$) according to the actual situation of the samples.

2.2.4. SEM petrography

A flat and smooth surface was prepared from original and each post-pyrolysis shale samples (without solvent extraction) for field emission scanning electron microscopes analysis. Argon ion beam polishing surfaces were obtained by argon ions using a Leica EM RES102 mill with an accelerating voltage of 8 kV, current of 2.8 mA, and about 8 h. A FEI Helios Nano lab 650 SEM was employed to obtain FE-SEM images. Detection modes included back-scattered electron (BSE) and secondary electron (SE). In this study, the DOM was first identified using mechanically polished blocks under an oil-immersed microscope with reflected white light and UV light (objective $50\times$). After identification and reflectance measurement, the DOM was examined using Ar-ion-milled blocks under SEM, based on their optical properties, e.g., occurrence, size dimension, unique morphology/shape and gray scale (Liu et al., 2017, 2022).

3. Results

3.1. Organic geochemical and petrological characteristics for original samples

As illustrated in Table 1, the shale sample has a TOC content of 8.01 wt%, and Tmax is approximately 446 °C. The original shale sample follows the maturation pathway of kerogen Type II on the hydrogen index versus Tmax temperature diagram (Fig. 3). According to the established conversion of $T_{\rm max}$ value to equivalent vitrinite reflectance (EqVR_o) by Jarvie et al. (2001), the EqVR_o is 0.87%, indicating that the studied sample is in mid-oil window maturity range (Table 1). Vitrinite reflectance values for the coal sample is less than 0.5% (Fig. 3).

The predominant dispersed organic matter (DOM) constituents in the LT-01 sample are abundant solid bitumen, chitinozoans, a few graptolites, vitrinite-like particles, bituminite, and small amounts of algae and liptodetrinite (Figs. 4 and 5). They can be recognized by their morphological characteristics, optical and



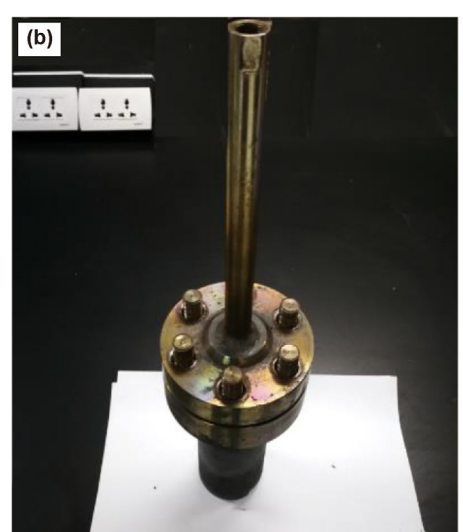


Fig. 2. Photographs to illustrate the anhydrous-pyrolysis equipment (a), assembled reactor with sample in jar (b).

fluorescent properties (Goodarzi et al., 1992; Suárez-Ruiz et al., 2012; Mastalerz et al., 2018; Spina et al., 2018; Gonçalves et al., 2024). A comparison of optical characteristics of chitinozoan, gratpolite, vitrinite-like particle and solid bitumen for maturity proxies are presented in Table 2.

Chitinozoans, occurring as single specimens, typically exhibit a median slit, smooth surface and a bulbous apex with long ornamental spines (Fig. 4(a) and (b)). They display partially compressed flask- or vase-like shapes (Fig. 4(c)), distinguished by a slender elongated form with thin walls surrounding the central cavity or pyrite-filled structures (Fig. 5(f)). Variations in shape, size, test wall thickness, and ornamental spines suggest the shale sample likely contains multiple chitinozoan species. The test walls exhibit uniform thickness with homogeneous and isotropic textures, contrasting with graptolites' characteristic fusellar layers and lathshaped structures (Fig. 4(d)). The framboidal pyrite fills void spaces within graptolite fragments. Graptolites in this study predominantly exhibit non-granular morphology. Both chitinozoans and graptolites are dark brown under UV light (Fig. 4(b) and (l)), and chitinozoan is more abundant than graptolite in the studied shale sample. Liptinite group was classified into mainly telalginite (Tasmanite cysts) (Fig. 4(f)-(h)), small quantity of residual liptodetrinite (Fig. 4(j)), and was recognized under UV light. It was observed that solid bitumen as stringy and fine-grained networks dispersed in mineral interstices or microfossils (Fig. 4(a)-(f), (i) and Fig. 5(c)–(e)). Filamentous solid bitumen occurs parallel to bedding (Figs. 4(c)-(f), (i) and 5(c)). Abundant scattered solid bitumen formed as small and fine irregular blobs, pore or fracture filling (Figs. 4(i) and 5(d)). The pre-oil solid bitumen with gray reflective surfaces and orange-brown fluorescence transitions, formed through telalginite transformation and thermal degradation, suggests a later oil generation in the maturation phase (Fig. 4(g)). Telalginite can be retained at higher maturity compared to lamalginite since it requires higher activation energies for degradation and oil generation (Glikson et al., 1992; Reyes et al., 2018). Generated oil with green fluorescence may be sorbed and retain in the carbonate nodule's surface (Fig. 4(j)). Carbonate minerals with oil inclusions can be examined (Fig. 4(b), (g) and (l)). A small quantity of VLPs were also recognized in this sample, exhibiting irregularly ellipsoidal or oval in sections perpendicular to bedding (discrete solitary particles), non-fluorescent or weakly fluorescent, and structureless in internal texture (Figs. 4(i)–(l) and 5(b)). The values of random reflectance for both types of OM are presented in Table 3. No discernible development of pores was identified in any individual DOM in the original shale sample (Fig. 5). Maceral examination of the co-matured CJZ coal sample demonstrates a composition dominated by vitrinite (90%), with subordinate inertinite (8%) and trace liptinite (2%) (Fig. 6(a)). Spores have hollow and yellow fluorescence, and are aligned with the bedding planes (Fig. 6(a) and (b)). Vitrinite reflectance measurements yield 0.44% for the untreated coal sample (Table 3).

3.2. Post-pyrolysis petrographic analysis

3.2.1. Reflectance and morphological evolution of DOM

With the increase in pyrolysis temperature, the random reflectance of graptolite, chitinozoan and solid bitumen, VLP and vitrinite increased (Table 3, Fig. 7). The CRo and GRo typically have overlapping reflectance values, and both are consistently higher than VLPRo and BRo at each pyrolysis temperature. The study found that chitinozoan and graptolite showed essentially little change at pyrolysis temperatures between 250 and 300 °C (Fig. 8), and no significant increase in DOM reflectance of shale pyrolysis residues was observed (Table 3). This possibly due to initial higher maturation or insufficient heating timeframes, which may have limited the change in reflectance with increasing pyrolysis temperature. Generally, GRo is slightly higher than CRo, yet highly reflecting diagenetic minerals contained within internal cavities of

Table 1Overview of geochemical and thermal maturity related parameters for original samples.

Sample	Depth, m	Lithology	TOC, %	S1, mg/g	S2, mg/g	HI	OI	ΡΙ	T_{\max} , °C	$VR_o/EqVR_o$, %
LT-01	2314.2	Shale	8.01	4.5	19.3	241	12	0.19	446	0.87
CJZ	/	Coal	63.17	0.41	72.21	114	26	0.01	425	0.44

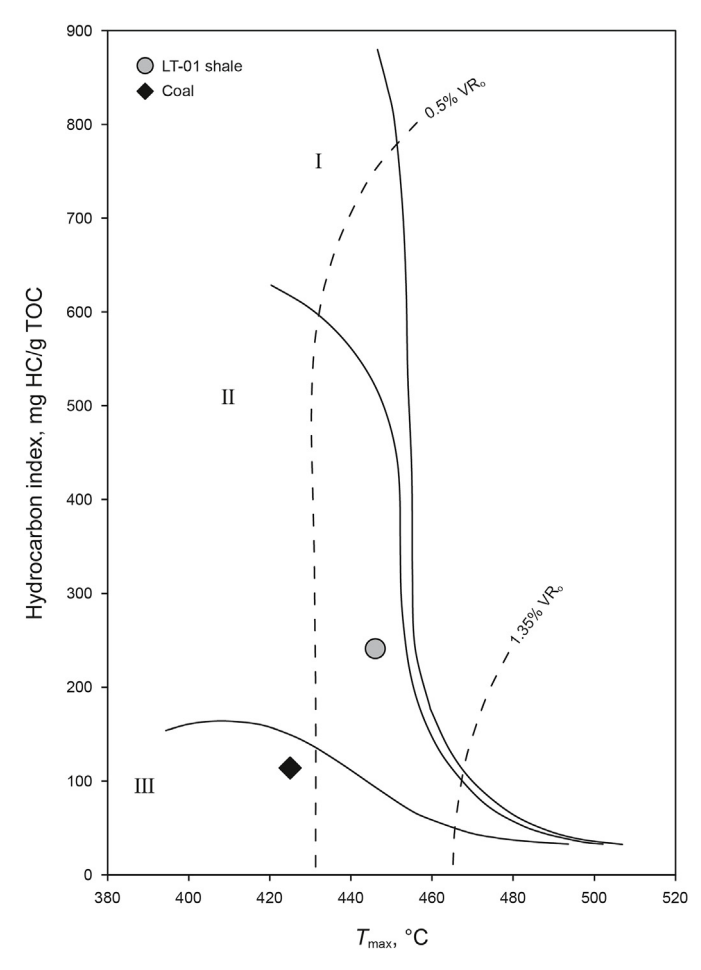


Fig. 3. Hydrogen index versus $T_{\rm max}$ (temperature of maximum S2 output) plot (Espitalié et al., 1985) showing kerogen types and thermal maturity of sample starting materials. HC: hydrocarbon; VR_o: vitrinite reflectance; TOC: total organic carbon.

chitinozoans may result in higher reflectance readings. At pyrolysis temperatures of 350 °C, the VLP surface developed a roughened granular texture (Fig. 9(h)), while devolatilization vacuoles and contraction fractures appeared in VLPs and solid bitumen (Fig. 9(e) and (i)). After anhydrous pyrolysis at 400 °C, chitinozoans and graptolites still maintain their primitive appearance (Fig. 10(a) and (d)), although thermal deterioration and granular anisotropy were observed in some graptolites (Fig. 10(e)). In contrast, the VLP develops fine-grained mosaic structures as well as new in-situ pores and cracks (Figs. 10(g)–(i) and 12(g)–(h)). Qualitatively, the relative abundance of solid bitumen decreased dramatically after 450 °C pyrolysis, creating pore spaces as the thermal simulation temperature rises. In residues from pyrolysis temperatures at 450–550 °C, the VLP displays an anisotropic and degassed character with a clearly visible fine grained mosaic microtexture (Fig. 11(c) and (f)), resulting in a slower rate of increase in its reflectance (Table 3, Fig. 7).

It should be noted that graptolites lacking define iconic features were not examined under the microscope in pyrolysis residues at 500 and 550 °C, which might be attributed to sample heterogeneity, and hence no GR₀ data were collected at advanced maturity level. A partially thermally degraded granular structure is observed at 500 °C pyrolysis (Fig. 11(g)). The development of pores and cracks along the fusellar layer of graptolite (Fig. 12(j)) reveals that it has some hydrocarbon generating capacity, consistent with prior studies (Luo et al., 2020; Zheng et al., 2021). Chitinozoans do not

appear differently between unheated materials and pyrolysis residues. They always have smooth boundaries, internal structureless and homogeneous surface (Figs. 8(d), 9(g), 10(d), and 11(a), (d), (e), (h)). The differences in morphological properties imply that this collection of chitinozoans may contain multiple distinct species. Chitinozoan thermally shrinks while retaining its unique original morphology without pronounced pores (Fig. 12(k) and (l)). Therefore, we can infer that chitinozoan is a relatively inert organic material compared to the other DOM. These findings imply that the chitinozoan is more resistant to thermal degradation than graptolite and VLP, which is supported by Reyes et al. (2018).

For vitrinite preserved in artificially co-matured coal samples, the color of vitrinite gradually changes from dark gray to grayish white as the pyrolysis temperature rises (Fig. 6). Contraction cracks and devolatilization vacuoles appear beyond 350 °C (Fig. 6(g)–(j)), consistent with reported bituminous rank of Wilcox Group coal (Mishra et al., 2022). Pore spaces created by complete thermal degradation of spores were observed after pyrolysis at 400 °C (Fig. 6(g)). No significant changes have occurred in inertinite between original materials and heated residues (Fig. 6). VRo increases gradually with the increase of heating temperature, and is 0.63%, 0.81%, 1.16%, 1.74%, 2.59%, 3.49%, 4.52% for 250, 300, 350, 400, 450, 500 and 550 °C, respectively (Table 3, Fig. 7). The VR_o slightly increases from original sample to 300 °C pyrolysis. The vitrinite in comatured coal heated after 350 °C has a significant and rapid VR_o increase. The VRo was significantly higher than CRo after pyrolysis 500 °C (Table 3).

3.2.2. Fluorecence intensity change of DOM

Green fluorescing hydrocarbon inclusions trapped inside the carbonate particles or filling voids were observed in original shale sample (Fig. 4(b), (g) and (l)), indicating oil generation and expulsion within shale. The observed yellow-orange fluorescent properties of the liptinite group from original sample indicated a relative thermal maturity near 0.8% EqVR₀ (Fig. 4(g), (h) and (j)), which is comparable to geochemical maturity data (Table 1) and is consistent with previous works for fluorescence evolution in Silurian Qusaiba shale (Cole, 1994). Alginate loses their morphology with simultaneous disappearance of the fluorescence at pyrolysis temperatures ranging from 250 to 300 °C. As pyrolysis temperature increased, the fluorescence properties of zooclasts gradually decreased. Until pyrolysis at 350 °C, chitinozoans and graptolites still display extremely dull brown fluorescence (Fig. 9(b) and (d)), but VLP and solid bitumen no longer have fluorescence (Fig. 9(f) and (j)). In fact, none of the chitinozoans are fluorescing (Reyes et al., 2018). This is mostly likely due to surface absorption of expelled hydrocarbon. All of the DOM in shale lose their fluorescence and show gradually thermal degradation after pyrolysis temperatures of 400 °C (Fig. 10). Spores in artificially co-matured coal are completely thermal degraded, and their fluorescence is very faint at 300 °C pyrolysis (Fig. 6(d) and (e)). They are entirely thermally deteriorated, and left small lenticular moldic spaces after 350 °C pyrolysis.

4. Discussion

4.1. Thermal evolution characteristics of DOM

4.1.1. The reflectance correlations between zooclasts, vitrinite-like particle and solid bitumen

Reyes et al. (2018) conducted a set of hydrous pyrolysis on a chitinozoan- and graptolite-bearing Upper Ordovician shale from the Hudson Bay Basin, Canada. Fig. 13 shows a comparison of the reflectances of graptolite, chitinozoan, solid bitumen, and vitrinite-like particle. Their results also exhibited that the random

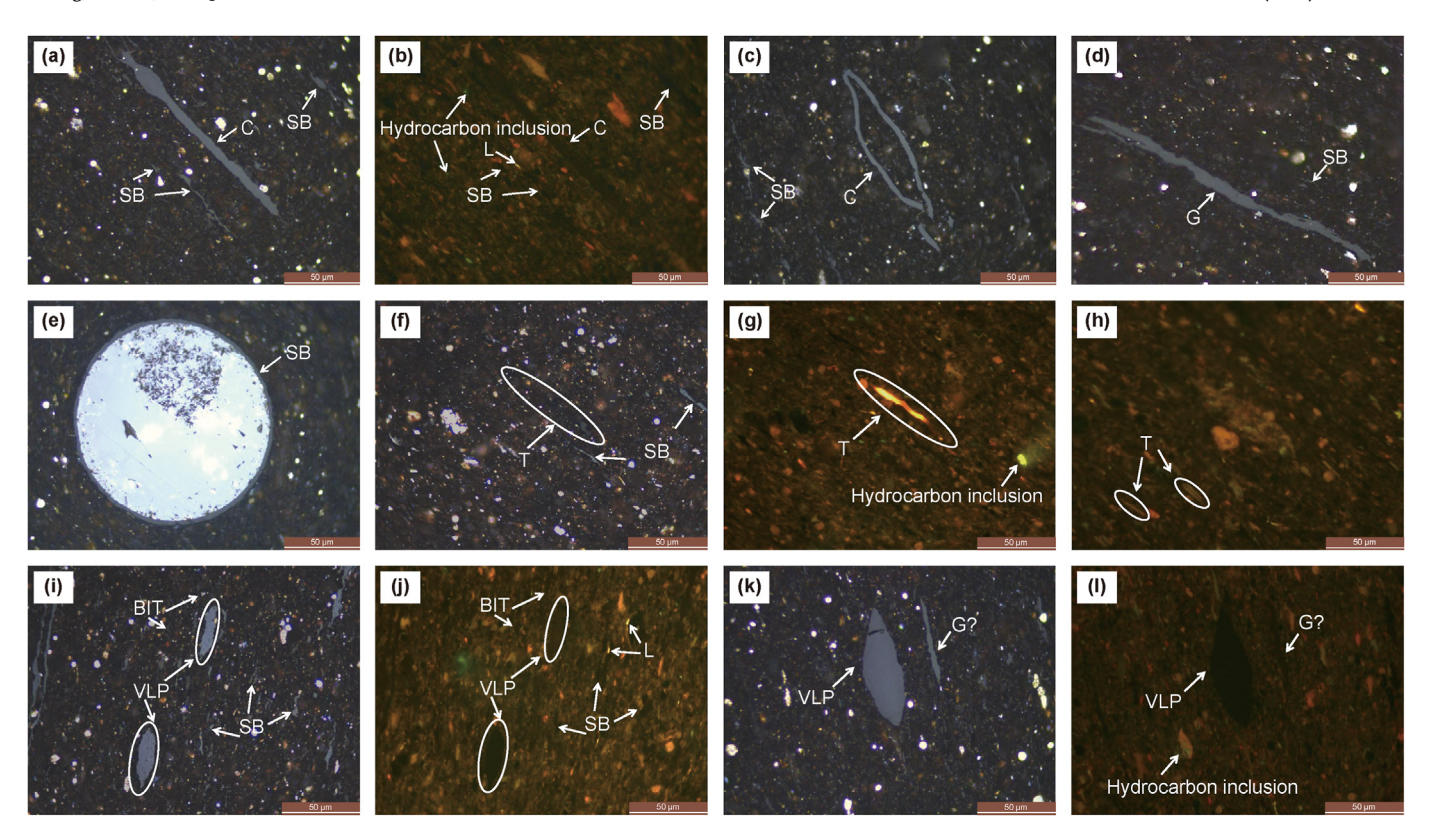


Fig. 4. Optical photomicrographs under oil immersion for LT-01 original shale sample.

(a-b) Chitinozoan (C) and solid bitumen (SB) with weak brown fluorescence, Liptodetrinite (L); (c) Chitinozoan (C) and solid bitumen (SB); (d) Graptolite (G) and solid bitumen (SB); (e) This is degraded siliceous spherical skeleton of Radiolarian replace with solid bitumen (SB). (f-g) Yellow-orange fluorescent long body of telalginite (T) undergo incomplete thermal degradation, and hydrocarbon inclusion; (h) Telalginite (T) with brown fluorescence; (i-j) Abundant solid bitumen (SB), bituminite (BIT), liptodetrinite (L), vitrinite-like particles (VLP) include one with dark brown fluorescence and another without fluorescence; (k-l) Vitrinite-like particle (VLP) without fluorescence, graptolite (G?) with weak brown fluorescence, and hydrocarbon inclusion.

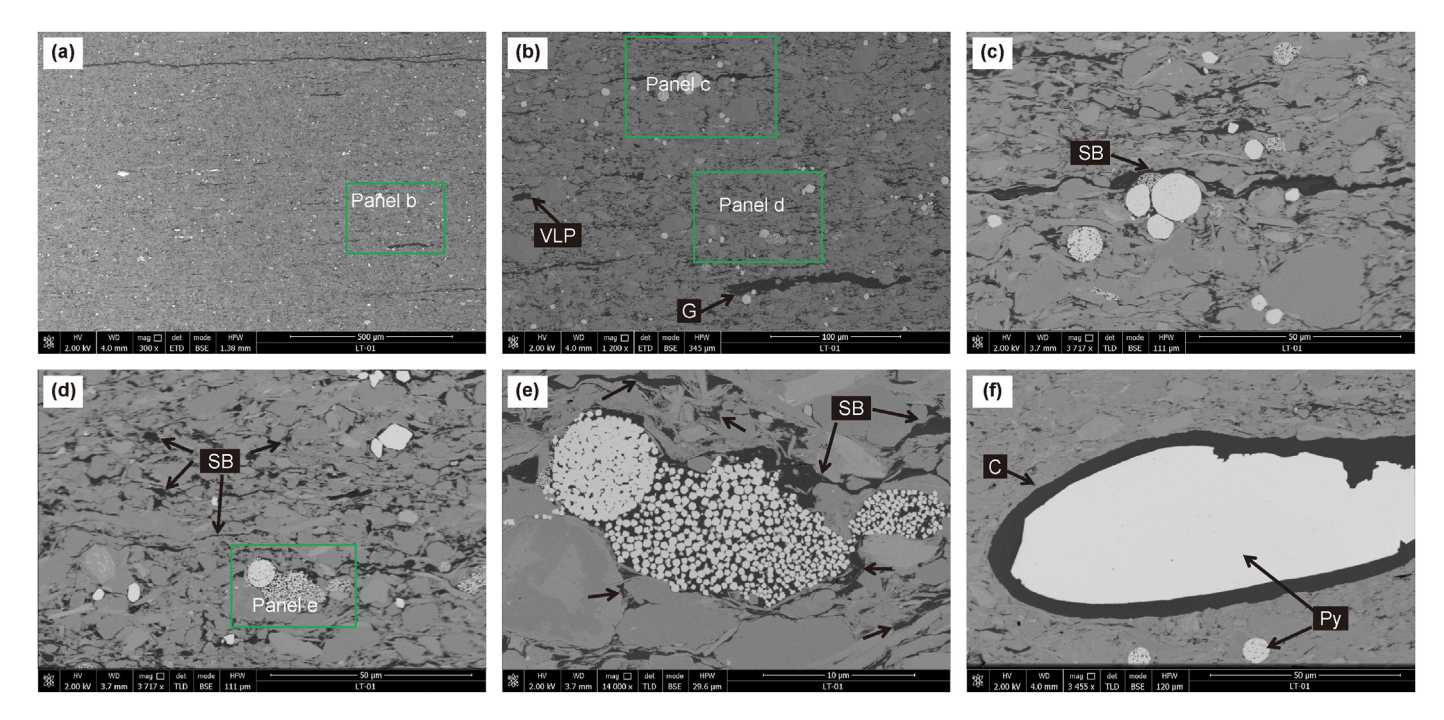


Fig. 5. SEM micrographs of the LT-01 original shale sample. (a) Ar-ion milled surface showing lamination, pyrite and distinct types of OM. Panels (b), (c), (d), and (e) are close-up views of the area bordered by green solid lines. VLP = Vitrinite-like particle; G = Graptolite; SB = Solid bitumen; C = Chitinozoan; Py = Pyrite.

Table 2Comparison of optical characteristics of chitinozoan, graptolite, vitrinite-like particle and solid bitumen for maturity proxies in the original sample LT-01 (modified from Goodarzi et al., 1992; Gonçalves et al., 2024; Luo et al., 2025).

Dispersed OM	Chitinozoan	Graptolite	Vitrinite-like particle	Solid bitumen
Origin	Original	Original	Original	Secondary
Occurrence	Single specimens, usually have slit in the middle, bulbous apex with long ornamental spines, partially compressed flask- or vase-like organic-walled structure and symmetrical along the central line	Complex biological structures with fusellar layers, common canal or thecae, and parallel periderm; Uniquely segmented and elongated shape in sections perpendicular to bedding	Irregularly ellipsoidal or oval shape (Discrete solitary particle) in sections perpendicular to bedding, aligning parallel to bedding plane	Pores and cracks-filling or embayment textures, occasionally parallel to bedding
Mineral inclusion	Surrounding the central cavity or pyrite	Sometimes filled with framboidal pyrite	Sometimes containing pyrite grains	Dispersed in clay minerals or microfossils (radiolarian)
Fluorescence properties	Dark brown to non-fluorescing	Dark brown	Faint brown to non-fluorescing	Reddish brown-weak brown
Surface feature	Smooth surface, homogenous	Smooth, consisting of lamellar layering with a fibrous structure	Smooth surface, homogenous texture	Smooth or less smooth surface
Size	Large	Large	$20{-}100~\mu m$ (lenths), $4{-}10~\mu m$ (widths)	Small

Table 3The results detail the reflectance determinations made on pre- and post-pyrolysis samples.

Temperature, °C	LT-01								CJZ	
	CR _o %	S.D. (N)	GR _o %	S.D. (N)	BR _o %	S.D. (N)	VLPR _o %	S.D. (N)	VR _o %	S.D. (N)
Original	0.82	0.05(5)	0.86	0.09(24)	0.54	0.13(65)	0.69	0.05(26)	0.44	0.03(43)
250	0.90	0.05(15)	0.87	0.05(27)	0.56	0.08(39)	0.75	0.05(10)	0.63	0.04(37)
300	0.86	0.02(26)	0.88	0.04(10)	0.71	0.11(47)	0.82	0.09(25)	0.81	0.04(40)
350	1.15	0.10(30)	1.31	0.09(35)	1.01	0.15(49)	1.04	0.06(32)	1.16	0.06(40)
400	1.95	0.07(16)	1.91	0.10(18)	1.47	0.22(53)	1.57	0.15(17)	1.74	0.09(38)
450	2.52	0.13(14)	2.43	0.10(8)	2.09	0.31(45)	2.47	0.38(16)	2.59	0.06(40)
500	3.16	0.16(11)	-	-	2.51	0.23(51)	2.60	0.30(14)	3.49	0.16(40)
550	3.77	0.27(13)	-	-	3.05	0.21(43)	2.79	0.29(16)	4.52	0.13(43)

CR₀%: random reflectance of chitinozoan; GR₀%: random reflectance of graptolite; BR₀%: random reflectance of solid bitumen; VLPR₀%: random reflectance of vitrinite-like particle.

S.D.: standard derivation; N: number of particles measured.

reflectance of graptolite and chitinozoan increased significantly with the rise in pyrolysis temperatures, which is consistent with the trend of our results (Fig. 13(a)). This suggests that zooclast reflectance exhibits the comparable thermal response regardless of thermal simulation methodology. Further, our results extend this tendency with different samples subjected to different experimental pyrolysis settings. Based on pyrolysis results of our experiment and Reyes et al. (2018), a linear regression equation of GR_0 and CR_0 can be expressed as:

$$GR_0 = 0.97CR_0 + 0.03 (R^2 = 0.98)$$
 (1)

Similarly, combined with their data, a series of reflectance relationships among the DOM can be expressed by the equations (Fig. 13(b)–(f)):

$$CR_0 = 1.13BR_0 + 0.26 (R^2 = 0.98)$$
 (2)

$$GR_0 = 1.02BR_0 + 0.33 (R^2 = 0.97)$$
(3)

$$CR_0 = 1.22VLPR_0 + 0.01 (R^2 = 0.95)$$
 (4)

$$GR_0 = 1.28VLPR_0 - 0.05 (R^2 = 0.97)$$
 (5)

$$VLPR_0 = 0.82BR_0 + 0.28 (R^2 = 0.95)$$
 (6)

The results show that positive linear correlations exist between the random reflectance of zooclasts and SB, except for VLP (Fig. 13). The correlation between $VLPR_0$ and BR_0 seems to be divided into two-stage linear regression (Fig. 13(f)).

The study also intends to determine if the maturation pathways of zooclasts in artificially matured materials are similar to those in naturally matured samples. Fig. 14 illustrates cross-plots of chitinozoan, graptolite and solid bitumen reflectances based on naturally matured series in Lower Paleozoic sediments. The statistical data reveal increasing dispersion with higher reflectivities owing to strong anisotropy at the advanced maturity stage. Linear regression equations can be expressed as (Fig. 14(a)—(c)):

$$GR_0 = 0.97CR_0 + 0.02 (R^2 = 0.95)$$
(7)

$$CR_0 = 0.99BR_0 + 0.16 (R^2 = 0.90)$$
 (8)

$$GR_0 = 1.11BR_0 + 0.07 (R^2 = 0.92)$$
(9)

Similar correlational relations remain between GR_0 and CR_0 in naturally and artificially matured settings (Figs. 13(a) and 14(a)). This suggests that zooclast reflectance is more stable and reliable. However, we note that the GR_0 demonstrates a higher level of maturity than BR_0 (Fig. 14(c)), yet the CR_0 was consistently slightly higher (Fig. 14(b)). Over a large maturity range, the GR_0 was frequently greater than BR_0 (Figs. 13(c) and 14(c)), indicating that graptolite has a higher degree of aromaticity (Song et al., 2023).

^{-:} No detection.

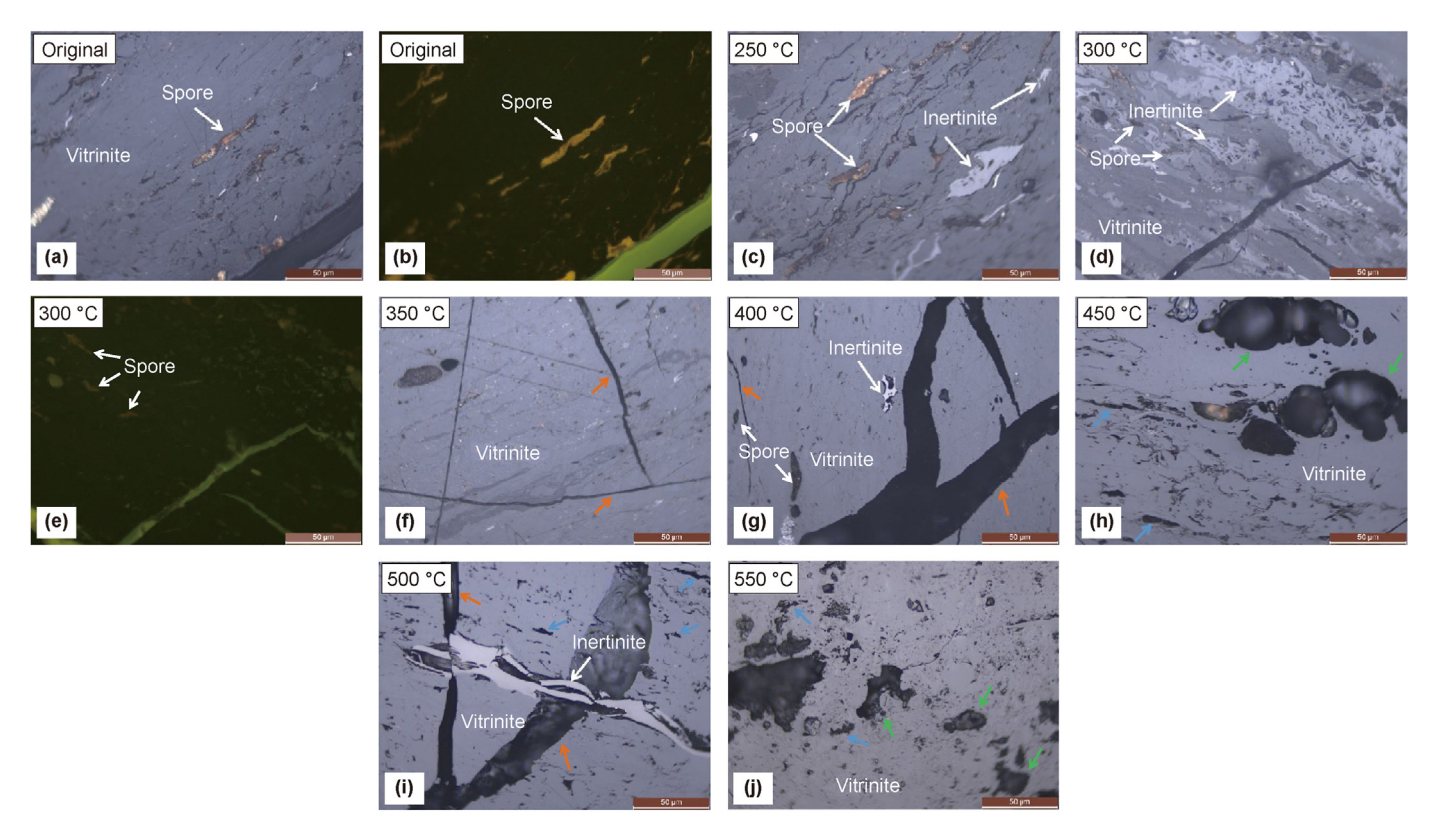


Fig. 6. Photomicrographs under oil immersion showing changes in original and artificial co-matured coal. (a—b) Vitrinite and spore with yellow fluorescence in original coal sample; (c) Vitrinite, inertinite and spore after pyrolysis at 250 °C; (d—e) Vitrinite and spore with faint brown fluorescence after pyrolysis at 300 °C; (f) Vitrinite after pyrolysis at 350 °C; (g) Vitrinite, inertinite and pore spaces created by uncompleted thermal degradation of spores after pyrolysis at 400 °C; (h—j) Small lenticular moldic spaces (blue arrow) left by thermally deteriorated spores. New and large bubble pores (green arrow) as well as cracks (orange arrow) in vitrinite were created after the artificial maturation from pyrolysis temperature of 350–550 °C.

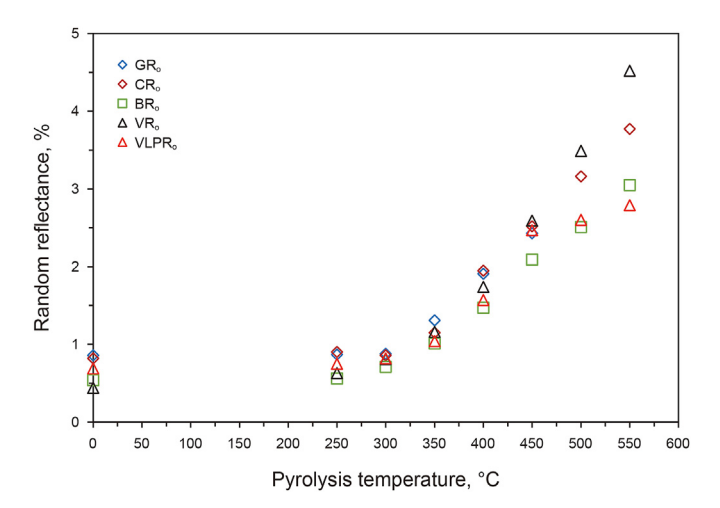


Fig. 7. Evolution of DOM random reflectances of coal and shale samples with increasing pyrolysis temperatures. Vitrinite reflectance (VR_o) for coal, CJZ. Graptolite reflectance (GR_o) , chitinozoan reflectance (CR_o) , solid bitumen reflectance (BR_o) , and vitrinite-like particle reflectance $(VLPR_o)$ for shale LT-01.

Statistically speaking, the range of maturity covered by the sample size impacts correlation. Maturity ranges up to 3% for the CR_0 and BR_0 in natural series (Fig. 14(b)). It can be difficult to obtain natural samples possessing a wide maturity range in the same basin or region, which have experienced normal burial maturation process and are likely to be influenced by thermal anomaly. However, the obtained BR_0 based on artificial pyrolysis experiments appears to

differ from geologically mature series (Figs. 13(b) and 14(b); Figs. 13(c) and 14(c)). The generation of solid bitumen and BR_0 evolution are significantly affected by pyrolysis conditions (Hackley et al., 2022). It is challenging to replicate the actual underground hydrocarbon generation and diagenesis process using the temperature and pressure conditions of a pyrolysis experiment. This difference is attributed to the aromatization degree of OM caused by the heating rate and maximum temperature in laboratory heating and natural geological burial maturation (Hackley et al., 2022), as well as the potential involvement of hydrothermal fluids in the processes (Schoenherr et al., 2007). These investigations suggest the existing empirical BR_0 conversion schemes should be applied with caution.

It is noteworthy that the VLPR₀ is applicable to reflectance less than 2.0%. Because as the pyrolysis temperature increases beyond 400 °C, the VLP develops markedly mosaics texture (Figs. 10(g) and 11(c)). Therefore, the valid range of VLP as a maturity proxy does not exceed 2% VLPR_o. This basic finding is consistent with what has been found in early hydrous pyrolysis of Middle Ordovician kukersite Estonian oil shale (Wang et al., 1996). Although the algal Gloeocapsomorpha prisca (G. prisca) is a typical feature and primary component of the Ordovician kukersites, no conclusive G. prisca was found in the studied sample. Wang et al. (1996) speculate that VLM is mainly derived from G. prisca and their degradation in situ residual products in Estonian oil shale. However, the result based on our work is inconsistent with that in Luo et al. (2021), which suggests that VLM can be used to determine the entire maturity stage of the Precambrian-Cambrian shales. This appears to indicate that VLP/VLM occurring in shales from different geological

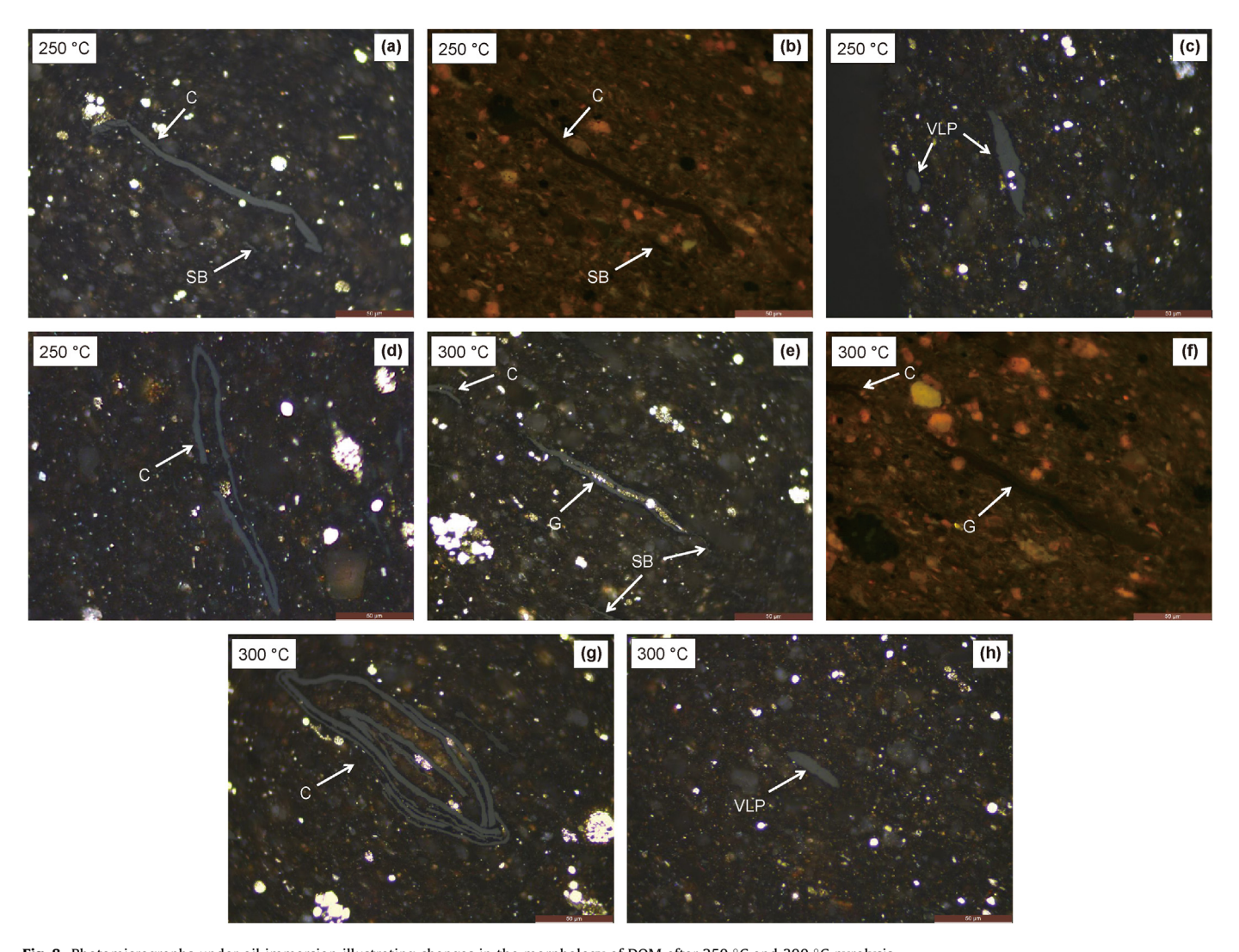


Fig. 8. Photomicrographs under oil immersion illustrating changes in the morphology of DOM after 250 °C and 300 °C pyrolysis. (**a–b**) Chitinozoan (C) with dull brown fluorescence and solid bitumen (SB) with little to no fluorescence; (**c**) Vitrinite-like particles (VLP); (**d**) Chitinozoan with vase-like shape; (**e–f**) Framboidal pyrite-filled graptolite (G) and stringy solid bitumen (SB); (**g**) Chitinozoan (C); (**h**) Vitrinite-like particles (VLP).

ages may have originated from distinct starting materials and different physiochemical evolution pathways during maturation.

4.1.2. The pitfalls of graptolite reflectance application

Graptolite reflectance has been used in numerous studies focusing on regional maturity (Luo et al., 2020 and related references). Researchers engaged in organic petrology have proposed various conversion equations based on GR₀ equivalent calculation (Goodarzi and Norford, 1987; Bertrand, 1990; Cole, 1994; Zhong and Qin, 1995; Petersen et al., 2013; Luo et al., 2018; Wang et al., 2019; Zheng et al., 2022). The low abundance of chitinozoan in samples has resulted in relatively few applications for evaluating maturity (Tricker et al., 1992). Previous studies initially confirmed correlation between VR_o and CR_o based on the coexistence of true collotelinite/ telinite and chitinozoan in collected samples from the late Silurian to Devonian sediments (Bertrand, 1990; Bertrand and Malo, 2001, 2012; Tricker et al., 1992), and further indicated the correlation among BR₀, GR₀ and other thermal indicators using CR₀ as a bridge link. Subsequently, some organic petrology researchers tried to establish the relationships between GRo and VRo via co-pyrolysis experiments of shale and coal (Bustin et al., 1989; Luo et al., 2018; Zheng et al., 2022). Such conversions would confront the

unresolved issue of the EqVR₀ not matching the geochemical thermal index, particularly with respect to the critical period of oil and gas generation (Zheng et al., 2022).

The random reflectance correlations between zooclasts and vitrinite may be determined by anhydrous pyrolysis. It should be emphasized that GR_o and CR_o do not exceed the initial maturity value when pyrolysis temperatures remain 250 °C for 48 h. This implies that peak burial temperature of the original sample is much higher than the combined starting temperature and duration used in the experiment. As a result, the data of original sample and 250 °C pyrolysis residues were excluded from the fitting relation. The correlations between VR_o and GR_o/CR_o can be expressed as, respectively (Fig. 15):

$$VR_0 = 1.13GR_0 - 0.27 (R^2 = 0.98)$$
 (10)

$$VR_0 = 1.24CR_0 - 0.39 (R^2 = 0.98)$$
(11)

Laboratory pyrolysis data overlap with natural evolution trend when CR_o is lower than 3.0% (Fig. 16). However, a notable discrepancy between artificial pyrolysis and natural evolution occurs after carbonization stage. The VR_o obtained by our pyrolysis

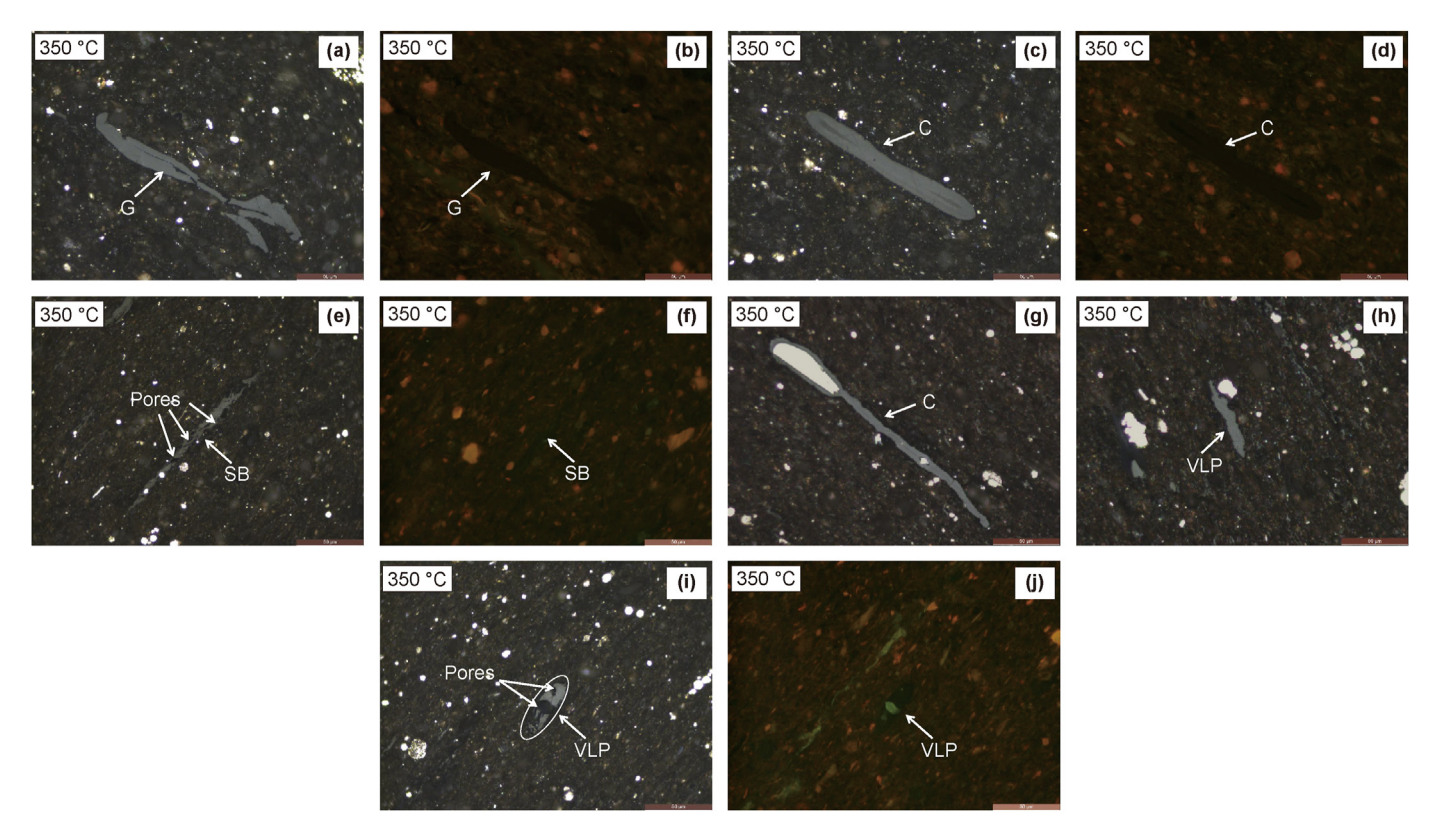


Fig. 9. Photomicrographs under oil immersion illustrating changes in the morphology of DOM after 350 °C pyrolysis. (\mathbf{a} - \mathbf{b}) Chitinozoan (\mathbf{C}) and Graptolite (\mathbf{G}) with extremely weak brown fluorescence; (\mathbf{c} - \mathbf{d}) Chitinozoan (\mathbf{C}) with extremely weak brown fluorescence; (\mathbf{e} - \mathbf{f}) The strip-shaped solid bitumen exhibits developed porosity and a roughened surface texture; (\mathbf{g}) Chitinozoan (\mathbf{C}) filled with pyrite; (\mathbf{h}) Vitrinite-like particle (VLP); (\mathbf{i} - \mathbf{j}) Vitrinite-like particle (VLP) develops contraction cracks and gas evacuation pores.

residues is higher than that of naturally matured samples (Bertrand, 1990; Tricker et al., 1992) (Fig. 16). After elevated pyrolvsis temperatures (450 °C), the differences between VR_o and CR_o increase (Fig. 7). This increased deviation may be attributed to VR_o suppression caused by high hydrogen content (Carr, 2000; Peters et al., 2018) in marine-influenced collotelinite/telinite in mixed marine and continental environments or to the differing maturation pathway (Bertrand and Malo, 2001; Bertrand, 1990). In addition, the original samples in this study were not oven-dried prior to pyrolysis, and may contain irreducible water in shale. Meanwhile, exogenous hydrogen released by structure water from clay mineral in shale may promote co-pyrolysis coal vitrinite maturation (Behar et al., 2003) during co-pyrolysis. It is important to emphasize that Jurassic coal was used for the co-matured coal in this study, as opposed to Carboniferous coals used in other investigations (Bustin et al., 1989; Luo et al., 2018; Zheng et al., 2022). This appears to be caused by the Jurassic vitrinite, which responds differently to thermal stress than vitrinite from Carboniferous coals.

Overall, the GR_o values presented here are in reasonable agreement with pyrolysis data reported previously (Bustin et al., 1989; Luo et al., 2018; Zheng et al., 2022) (Fig. 17). However, the data points are more scattered at higher pyrolysis temperatures/ maturity levels, and this spread is more evident for reflectance higher than 3.5%–4%. Based on laboratory simulated maturation, Bustin et al. (1989) proposed that the graptolite random reflectance is similar to the vitrinite random reflectance. Luo et al. (2018) conducted thermal simulation experiments using two low-maturity Alum shales. The results of one Alum shale pyrolysis experiment show that graptolite random reflectance in sections perpendicular to bedding were highly comparable to ours (Fig. 17).

This suggests that the random reflectance of graptolites measured on perpendicular to bedding increases at a steady rate as experimental temperature rises. It seems that kerogen-concentrated polished blocks are preferred in past studies. Bustin et al. (1989) evaluated random reflectance in polished pellets and reported that it was largely in portions adjacent to or parallel to bedding, which is similar to Bertrand's (1990) results for polished slide kerogen concentrates. Zheng et al. (2022) measured random reflectance without consideration of sections perpendicular to bedding in pellets of the solid residues following hydrous gold tube pyrolysis of Alum shale and observed an anomalous breakdown in the gradient of graptolite reflectance. This phenomenon is attributed to the influence of nanopores generated during hydrocarbon generation processes, which alter the reflectance of graptolites. Similarly, we observed that pores and cracks preferentially develop along the inner fusellar layers within graptolite during pyrolysis (Fig. 12(e) and (j)).

The possible reasons for the differences in empirical equations include: (1) Sample preparation. A major problem with graptolite reflectance application is the orientation of measurement (Malinconico, 1993). In most studies, reflectance measurements were performed on polished concentrates of kerogen (Bertrand, 1990; Yang and Hesse, 1993; Cole, 1994), crushed pellets (Petersen et al., 2013; Reyes et al., 2018; Zheng et al., 2022), and sections in parallel (Riediger et al., 1989) or perpendicular to the bedding (Luo et al., 2018; Wang et al., 2019; Cichon-Pupienis et al., 2020). It does not however take into account the differing morphology of the graptolite fragments being measured such as the granularity and sample preparation. It also does not take into account the biases of the person taking the measurement.

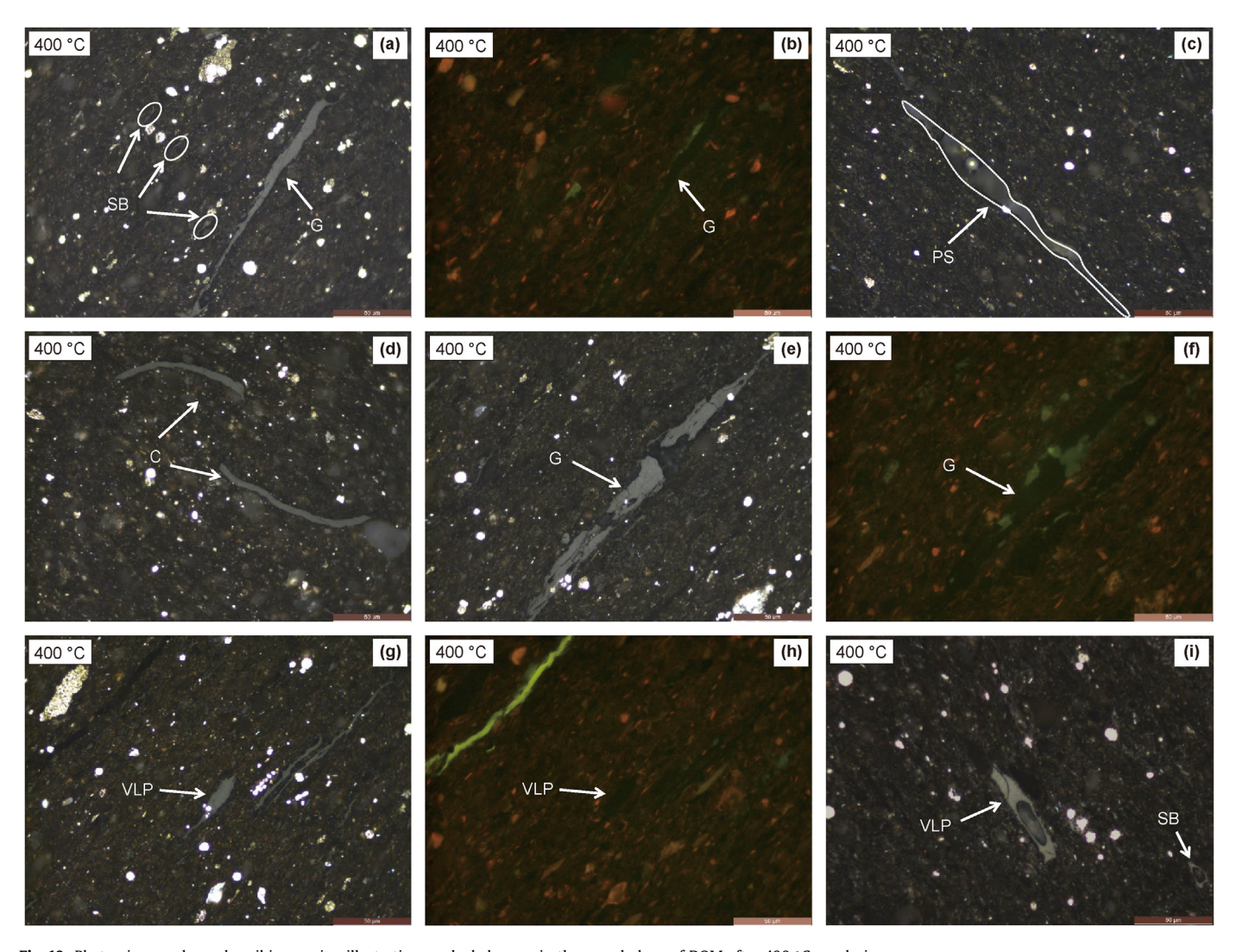


Fig. 10. Photomicrographs under oil immersion illustrating marked changes in the morphology of DOM after 400 $^{\circ}$ C pyrolysis. (a-b) Graptolite (G) exhibits minor thermal degradation and loss of fluorescence, accompanied by filamentous solid bitumen (SB); (c) Pore space (PS) or moldic pore is created by almost full conversion of telalginite or bituminite; (d) Chitinozoan (C) fragments; (e-f) Graptolite (G) exhibits thermal degradation and loss of fluorescence, with morphological alterations concentrated along marginal zones and within the inner fusellar layers; (g-h) Vitrinite-like particle (VLP) exhibits a rough and granular surface morphology with absence of fluorescence features; (i) Vitrinite-like particle (VLP) shows a fine-grained mosaic texture in optical properties, accompanied by contraction cracks and gas evacuation vacuoles formed during pyrolysis. The coated solid bitumen (SB) occurs with quartz, forming an elliptical ring.

Graptolites, as optical biaxial property materials, have significant anisotropy that increases with thermal maturity levels (Malinconico, 1993). Moreover, anisotropy depends on orientation of the polished block to the bedding. Its anisotropy is more pronounced in sections parallel to bedding than sections perpendicular to bedding. In sections parallel to bedding, distinct fusellar layers with alternate dark and bright interior structures are easily visible (Goodarzi et al., 1985; Wang et al., 2019). (2) Identification of graptolite. Graptolite particles lacking diagnostic features and exhibiting lenticular shape will not be easily distinguished from VLP (Petersen et al., 2013). (3) Graptolite species and fractions. Graptolite species (classification) do influence the reflectance values as well as conversion relations (Hartkopf-Fröder et al., 2015; Luo et al., 2018). Moreover, thermal maturation may cause variable responses in various graptolite fractions. Different anatomical fractions of graptolite have distinctive potential for hydrocarbon generation due to their diverse organic geochemical compositions (Zheng et al., 2021). The random reflectance data of graptolite in low grade regional metamorphism are extremely scattered when

the orientation of polished blocks is ignored (Malinconico, 1993), which presents a challenge for drilling cuttings, crushed particles or kerogen concentrates (Wang et al., 2021). (4) Sedimentary environmental conditions can affect zooclast reflectance (Cole, 1994). (5) Reflectance suppression. Graptolite reflectance suppression (Goodarzi et al., 1985) by surface imperfection induced by secondary nanopores generated by hydrocarbon gas generation in certain parts of graptolite tissue (Zheng et al., 2021). On the contrary, CR₀ typically does not show significant suppression (Tricker et al., 1992). Chitinozoan exhibit relief, are easily recognized (avoiding the problem of particles identification), and are isotropic when compared to graptolites via pyrolysis experiment. The graptolites develop visible secondary organic pores, leading to defects in the measuring surface. Compared to the other DOM, chitinozoan is more resistant to thermal degradation after the 400 °C stage of pyrolysis. Perpendicular sections allow chitinozoan to be recognized with high readiness and certainty. As a result, chitinozoan could be used in preference to graptolite. Future work should consider interlaboratory studies conducted on petrographic

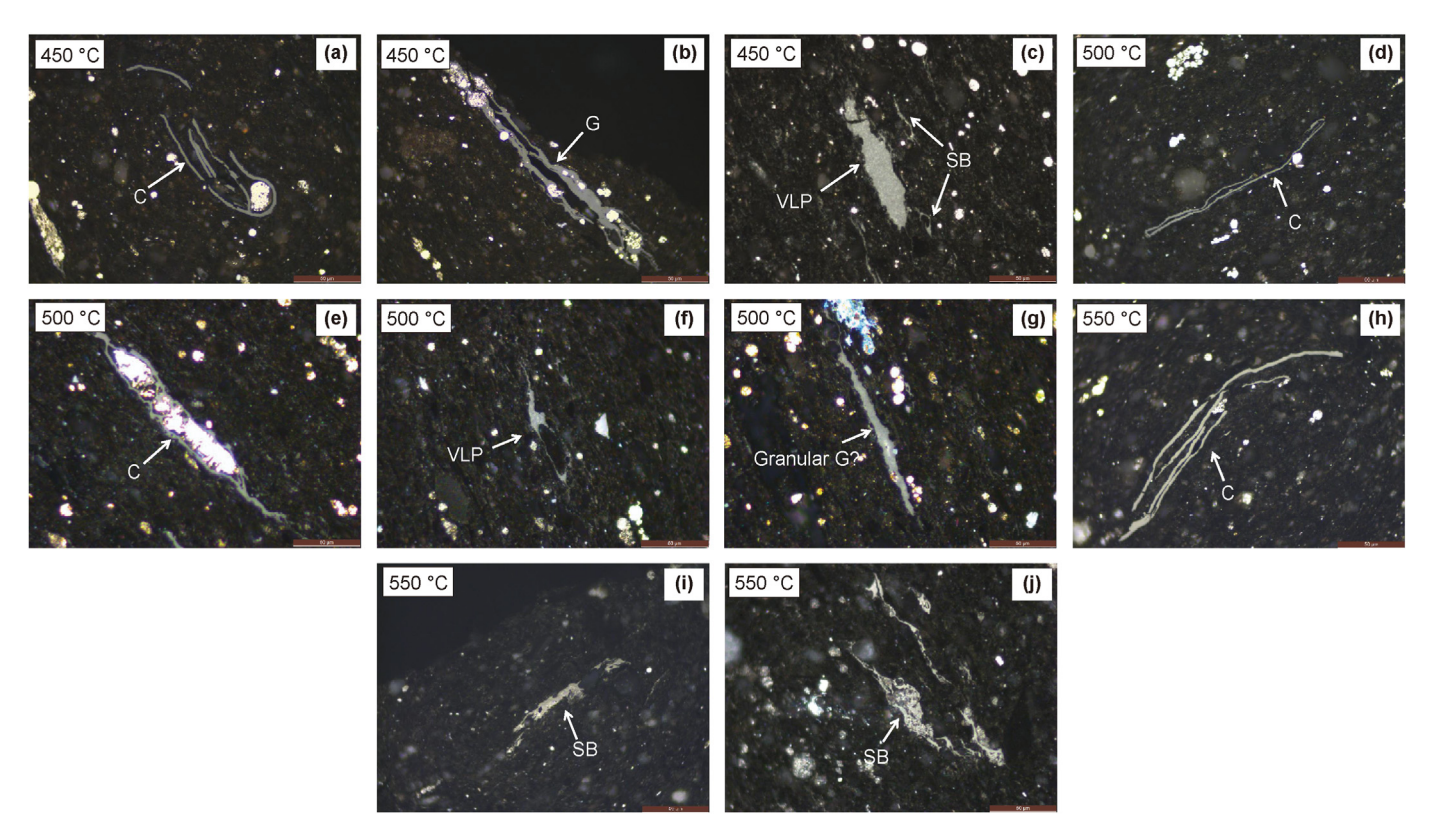


Fig. 11. Photomicrographs under oil immersion illustrating changes in the morphology of DOM after 450, 500 and 550 °C pyrolysis.

(a) Thin-walled chitinozoan (C); (b) The void spaces within graptolite (G) framework are filled with framboidal pyrite; (c) A fine-grained mosaic developed in vitrinite-like particle (VLP); (d–e) Thermal shrinkage along the edges of chitinozoan (C); (f) Vitrinite-like particle (VLP) exhibits a fine-grained mosaic texture, along with a gas evacuation vacuole; (g) Granular graptolite. We speculate that it is transformed from graptolite (G?) with weak brown fluorescence (see Fig. 4(k) and (l)); (h) Thermally induced contraction features along the edges of chitinozoan (C); (i–j) Anisotropic solid bitumen (SB).

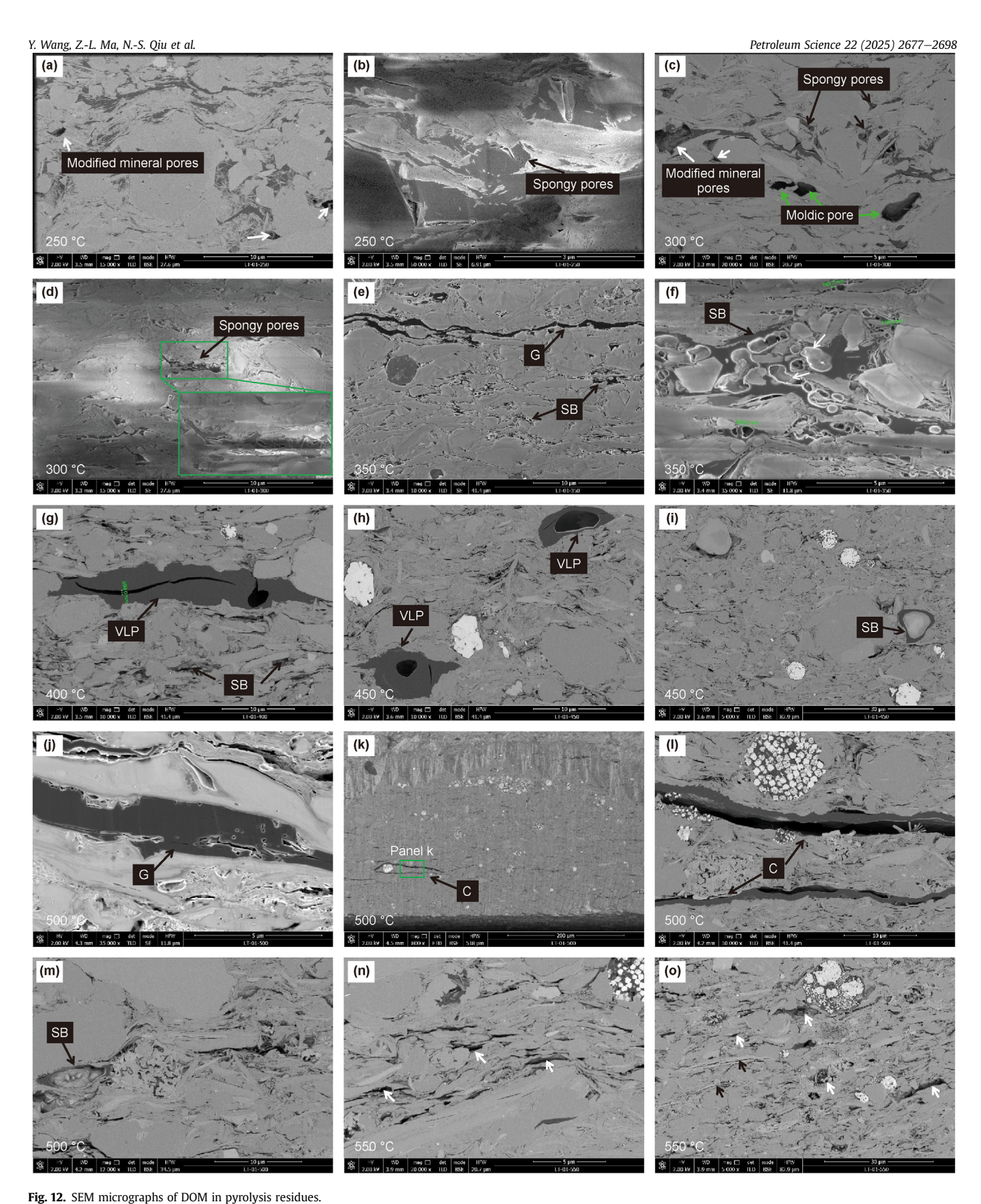
distinction as well as test standardization and reproducibility of zooclasts reflectance measurements.

4.2. Differences in the thermal evolutionary behavior of vitrinite-like particle and solid bitumen

With increasing experimental temperature, the color for both VLP and SB ranged from dark gray to grayish white (Figs. 4, 8–11). The reflectances of VLP and SB demonstrate a somewhat different path as temperatures increase (Fig. 7). The VLPRo and BRo do not increase significantly from original materials to 300 °C pyrolysis residues (Table 3). The reflectance of VLP is higher than those of SB except at the pyrolysis temperature of 550 °C. At temperatures below 450 °C, both VLPR₀ and BR₀ experienced modest increases in reflectance. At temperatures above 500 °C, BRo demonstrated a noticeably higher rate of increase than VLPR₀, and eventually reached a reflectance of 3.05% at 550 °C. The VLPR_o at 550 °C was 2.79%. It is important to note that the VLPR₀ and BR₀ values in anhydrous residues appear to be systematically lower than VR₀ of co-matured coal after 400 °C. A possible explanation is that the presence of hydrogen donated from structural water in clay minerals release (Klaja et al., 2020) during pyrolysis may favor a radical disproportionation mechanism which promotes newly generated solid bitumen (Hackley et al., 2022). Additionally, exogenous hydrogen derived from water may facilitate the vitrinite maturation reaction (Behar et al., 2003). The combination of these two factors has resulted in a low BR₀ of recovered shale pyrolysis residues after pyrolysis at 450 °C, which is notably lower than VR_o of co-matured coal. It should be mentioned that the presence of irreducible water

cannot be ruled out since the original samples were not oven-dried prior to pyrolysis.

SEM imaging analysis reveals that none of the specific DOM host pores were observed in original shale sample, apart from slit-like pores (Fig. 5), which occur between OM and mineral grain boundaries that likely reflect artefacts of sample preparation or desiccation (Fishman et al., 2012) or microfracture formed by oilgeneration (Berg and Gangi, 1999). Minor alginate or liptodetrinite particles were first thermally degraded (Fig. 12(a)). Nanometer-sized spongy pores started to appear within SB or bituminite at 250 °C and 300 °C (Fig. 12(b)-(d)). The size and number of these spongy pores increase with pyrolysis temperature, allowing them to connect to form bubble pores (Fig. 12(d)–(f)). Some isolated particulate OM (algae or liptodetrinite) <1 μm in size was converted to oil, leaving large moldic spaces (Fig. 12(c)). As we can see in Fig. 10(c), moldic pore is created by almost full thermal degradation of telalginite or bituminite. Following pyrolysis after 350 °C, VLP begins to show gradual morphology changes caused by devolatilization, exhibiting contraction cracks and gas evacuation vacuoles (Figs. 9(i), 10(i), 11(c) and 12(g)–(h)). The devolatilization pores are rounded or elliptical, with diameter of less than 10 μm , resembling vitrinite (Fig. 6(h)-(j)). Also, pronounced fine-grained mosaic texture appears in the optical properties (Figs. 10(i) and 11(c), (f)). The interpretation of reflectance analysis indicates that the optical properties of VLP are mostly related to maturity. Likewise, cracks and micrometer-sized, bubble-shaped OM-hosted pores began to form in the VLP, as observed via SEM analysis (Fig. 12(g) and (h)), possibly related to the greater amounts of generated gas (Ko et al., 2016). After 500 °C pyrolysis, modified mineral pores with relic OM were the most abundant type, while



(a) Modified mineral pores (white arrow) were derived from algae or liptodetrinite degradation; (b) OM-hosted spongy pores were developed in the solid bitumen; (c) Spongy

pores (black arrow) and modified mineral pores (white arrow). Algae or liptodetrinite is converted to oil, leaving large moldic pores (green arrow); (**d**) OM spongy pores (black arrow) in the solid bitumen; (**e**-**f**) OM bubble pores developed within solid bitumen. Graptolite shows no pore development as viewed in the SEM; (**g**-**h**) Vitrinite-like particles (VLP) develop contraction cracks and gas evacuation pores; (i) The coated solid bitumen (SB) occurs with quartz, forming an elliptical ring; (j) Development of pores and cracks in graptolite (G); (k-I) Chitinozoan thermally shrinks while retaining its original unique morphology without visible pores; (m) The coated solid bitumen (SB) occurs with secondary carbonate crystals, forming an elliptical ring; (**n-o**) Abundant modified mineral pores with relic solid bitumen (white arrow). Clay-mineral intergranular pores (black arrow).

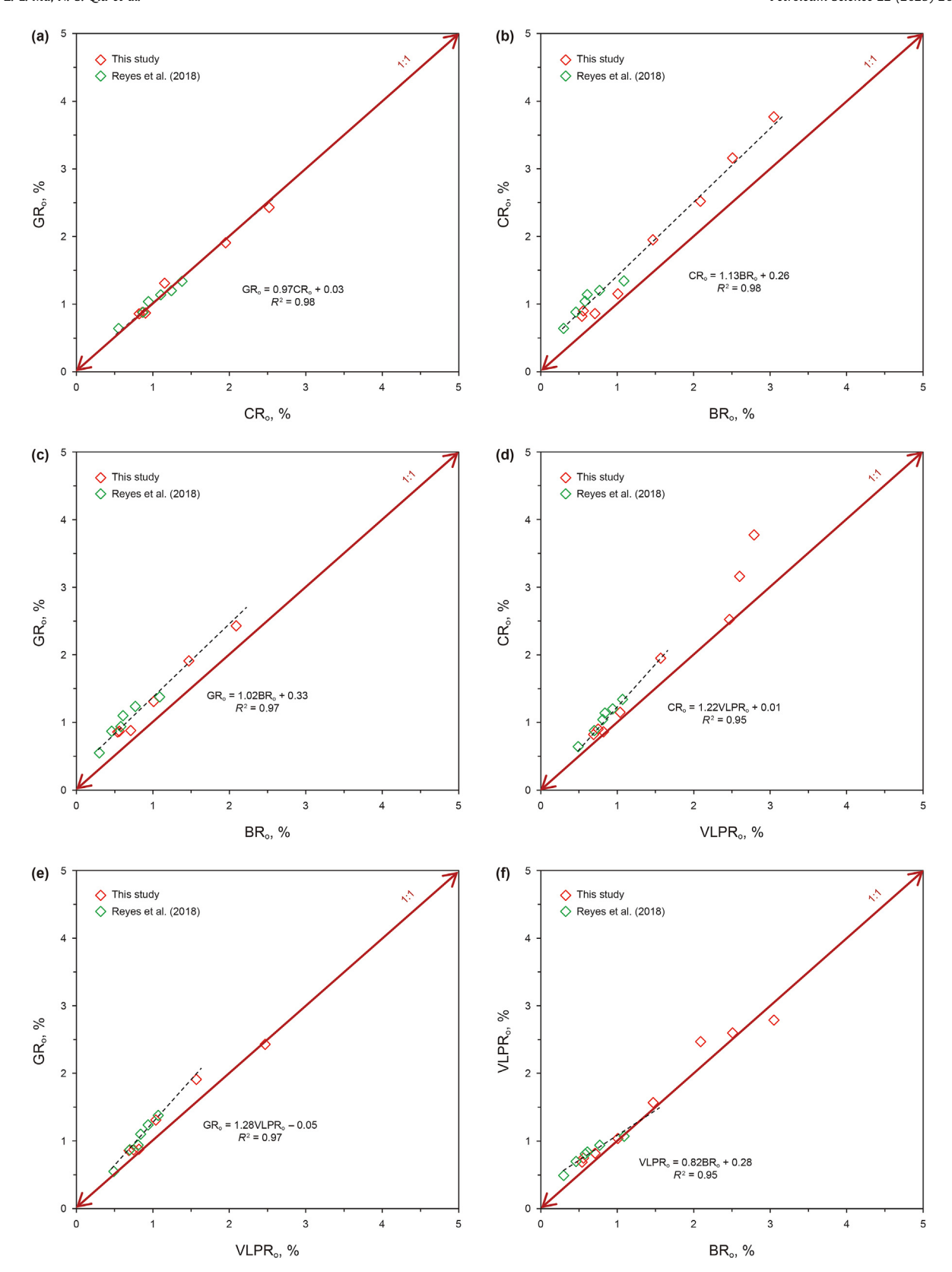


Fig. 13. Comparison among the reflectances of graptolite, chitinozoan, solid bitumen and vitrinite-like particle under hydrous and anhydrous pyrolysis conditions.

(a) Cross plot of GR₀ vs. CR₀; (b) Cross plot of CR₀ vs. BR₀; (c) Cross plot of GR₀ vs. BR₀; (d) Cross plot of CR₀ vs. VLPR₀; (e) Cross plot of GR₀ vs. VLPR₀; (f) Cross plot of VLPR₀ vs. BR₀.

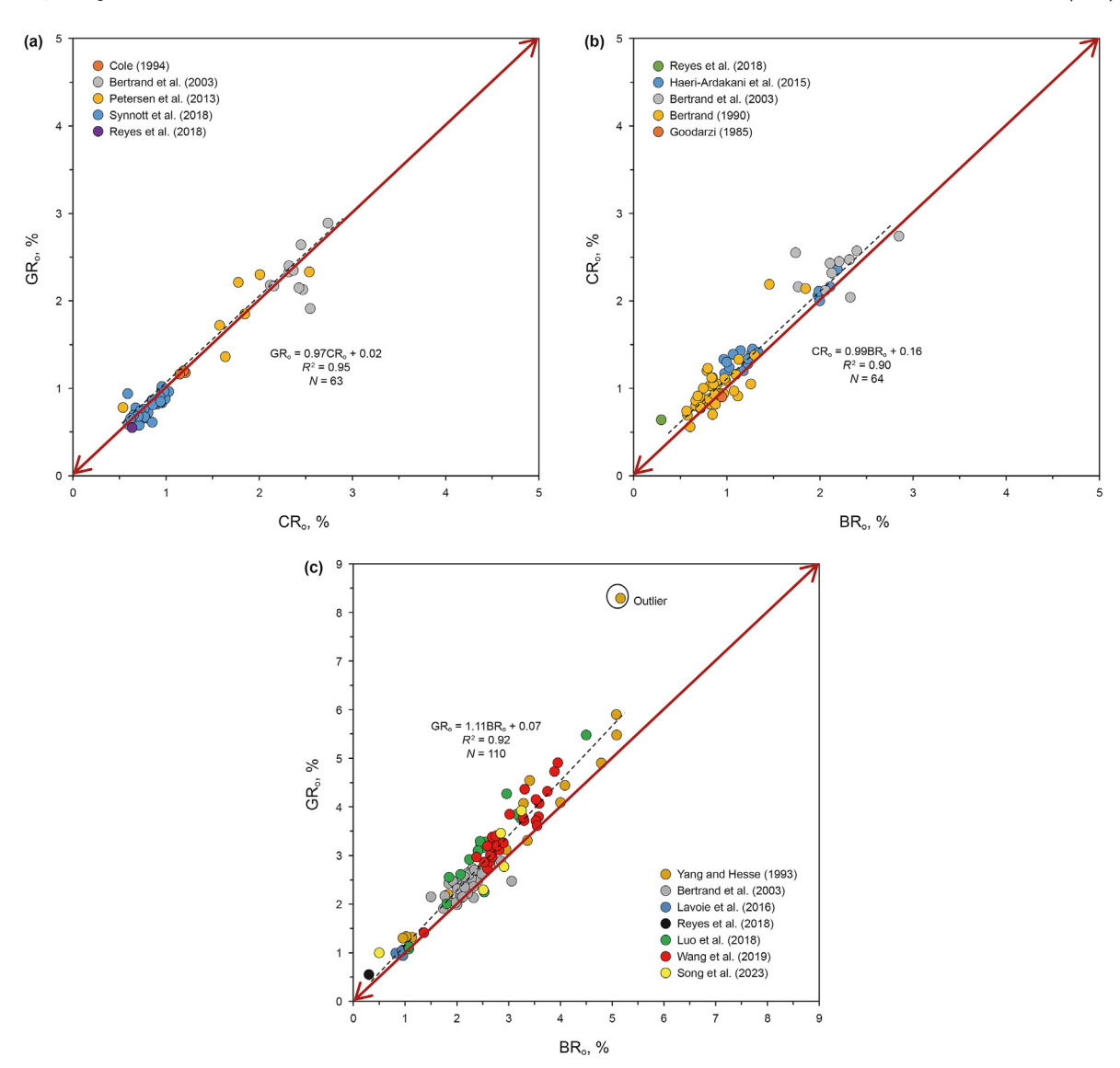


Fig. 14. Reflectance relationships among graptolite, chitinozoan, solid bitumen and vitrinite-like particle are established based on analyses of naturally matured series. (a) Cross plot of GR₀ vs CR₀; (b) Cross plot of CR₀ vs BR₀; (c) Cross plot of GR₀ vs BR₀.

modified interparticle pores between clay mineral platelets and intraparticle pores between clay mineral and OM were also commonly observed (Fig. 12(j)-(o)). These pores may result from oil migrating in mineral pores and/or leaving mineral pores, leaving behind a rim of cracked residual solid bitumen (Ko et al., 2018). The coated SB occurs with quartz or secondary carbonate crystals, forming an elliptical ring (Fig. 12(i) and (m)). This might represent newly generated SB, considering that it was not discovered in the original sample. The optical properties of the VLP vary from isotropic to markedly anisotropic as the pyrolysis temperature increases (Figs. 4(k), 8(c), 9(h), (i), 10(g), (i), and 11(c), (f)). Based on evidence of the optical texture and organic pore evolution, we argue that a fair amount of VLP in Upper Ordovician shale sample from the Baltic Basin, Lithuania does not consist of graptolite-type fragments. Yet this does not rule out the possibility that VLP is graptolite fragment in graptolite-rich shales (Luo et al., 2025).

To further investigate correlation between VLPR_o and BR_o in artificially matured residues (via pyrolysis) and naturally matured series, we provide a comparison between the findings of our study and earlier researches (Figs. 18 and 19). Fig. 18 shows the reflectance

results from artificial maturation series of vitrinite-like materials and solid bitumen (Wang et al., 1996; Xiao et al., 2000; Hackley and Lewan, 2018; Reyes et al., 2018; Luo et al., 2021). The VLPRo follow the BR_o versus temperature pattern, indicating that they most likely represent a type of solid bitumen (Fig. 18(a)–(c)). In contrast, the VLM in Alum shale follows the VRo versus temperature trend (Fig. 18(d)). Fig. 19 illustrates a cross-correlation analysis between BRo and VLPRo, systematically comparing their trends in naturally matured geological samples and artificially pyrolyzed residues. When the BR_o and VLPR_o values fall below 1.2%, our data overlaps with naturally Ordovician source rocks from Tarim Basin (Xiao et al., 2000) and artificially matured Upper Ordovician shale from Hudson Bay Basin (Reyes et al., 2018). Surprisingly, the measured VLPR₀ in naturally mature Alum shale was anomalously higher than BR_o according to Petersen et al. (2013) (Fig. 19). Xiao et al. (2000) identified a non-linear correlation between BRo and VLPRo in naturally mature samples, while Luo et al. (2021) demonstrated a distinct linear relationship within anhydrous pyrolysis residues of Cambrian Alum shale. Notably, Petersen et al. (2013) proposed that solid bitumen in their examined Alum outcrop samples may have

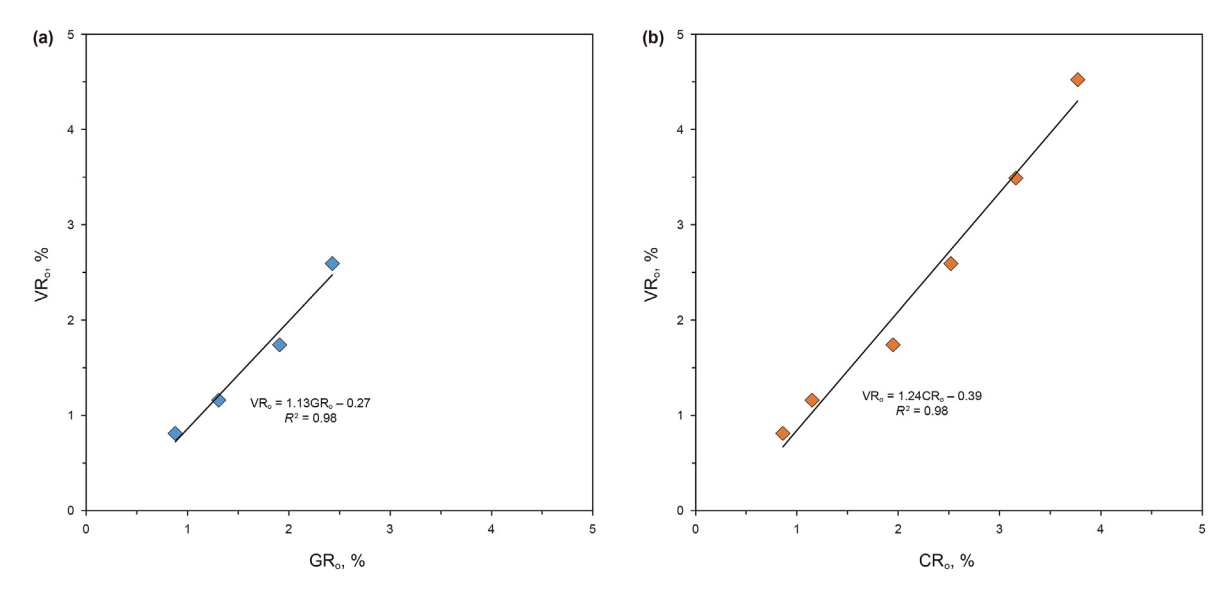


Fig. 15. Relationships between zooclast reflectance and vitrinite reflectance obtained from anhydrous pyrolysis experiments. (a) GRo vs VRo; (b) CRo vs VRo.

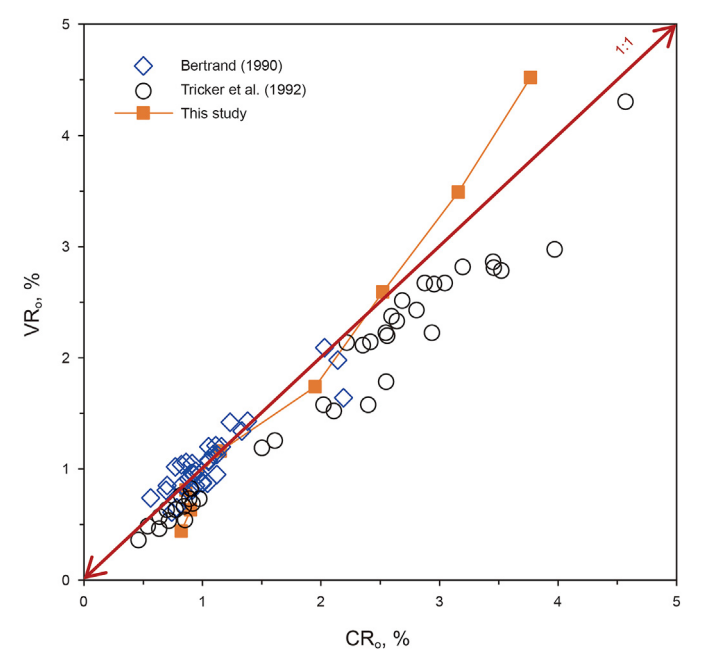


Fig. 16. Comparison for random reflectance of vitrinite and chitinozoan between artificial pyrolysis and natural thermal evolution.

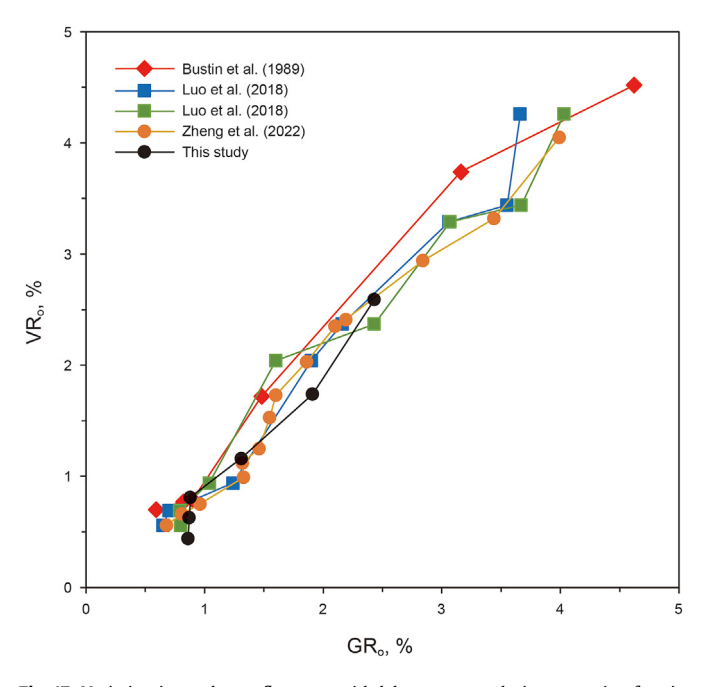


Fig. 17. Variation in random reflectance with laboratory pyrolysis maturation for vitrinite and graptolite.

been formed by biodegradation of oil or from deasphalting, rather than being thermogenic mechanism. Consequently, such solid bitumen cannot be utilized to determine thermal maturity. Our correlation between BRo and VLPRo was similar to Xiao et al. (2000), which indicates that the correlation of their thermal maturation pathways exhibits stage-specific characteristics and patterns, except for the Alum shale pyrolysis residues (Fig. 19). At equivalent maturity level at equivalent maturity levels compared to other studies, Alum shale has the highest reflectance of VLP (Fig. 19). The VLPRo-BRo correlations observed in artificial mature Mesoproterozoic Xiamaling shale and Cambrian Alum shale (Luo et al., 2021) are significantly different from in the studied Ordovician samples. This implies that the VLP, despite their similar morphology, may have originated from diverse starting materials (kerogen precursor)

in different geological periods and may have been influenced by thermal anomalies during evolution.

The LT-01 sample pyrolysis residue exhibits the development of a fine-grained mosaic texture in VLP, which is correlated with high temperatures and heating rates. Compared to the observation in artificially developed Cambrian Alum shale, this is substantially different. Specifically, the overall OM in uranium-enriched Alum shale has been greatly affected by uranium irradiation (Yang et al., 2019). These VLMs may have been affected by radiation, leading to random processes of aromatization and polymerization (Dahl et al., 1988; Yang et al., 2019). Furthermore, we examined the VLP in Alum shale and visually assessed that they are more solid and dense (Wang et al., 2020). Due to high uranium content bombarding the α -particles, molecular structure of VLP becomes more aromatic at

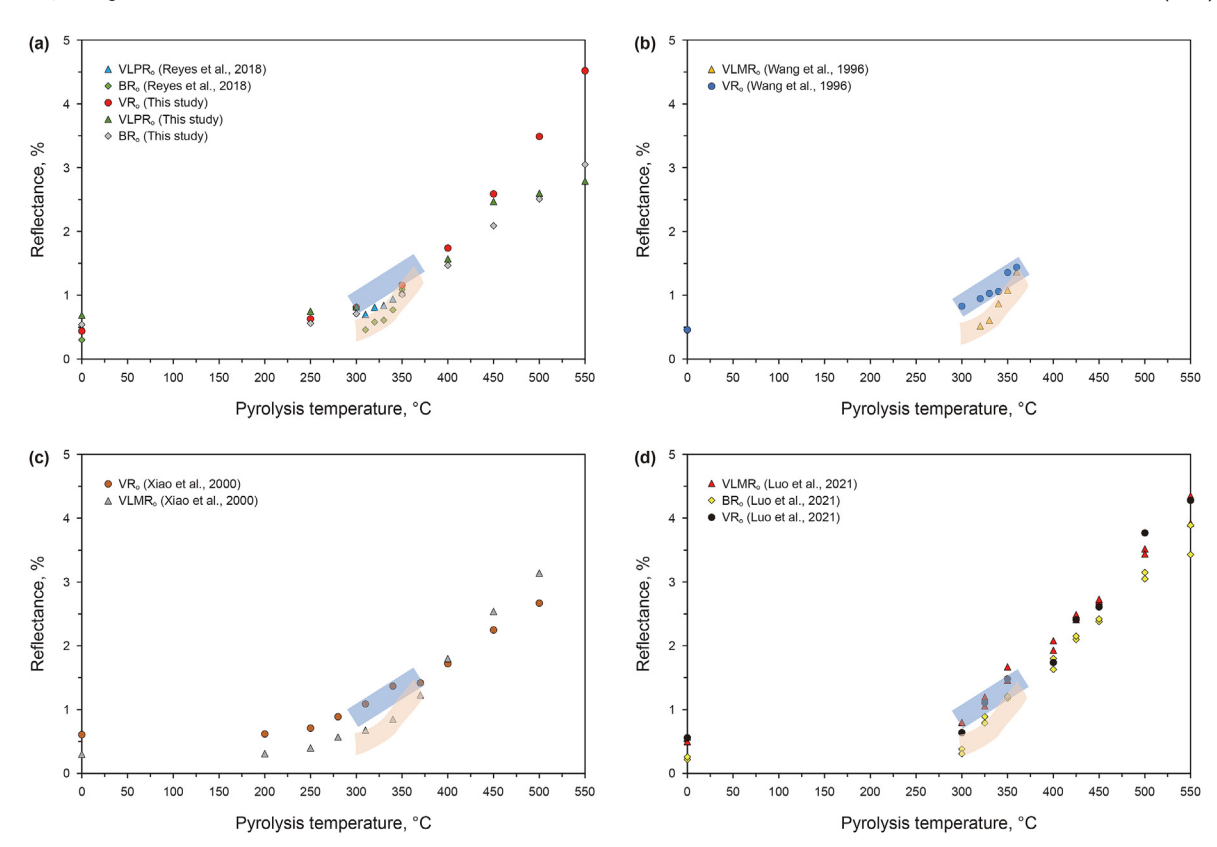


Fig. 18. Comparison of random reflectance variations of vitrinite, solid bitumen and vitrinite-like material with increasing pyrolysis temperature. The shades of blue and orange represent vitrinite and solid bitumen trends, respectively (modified after Hackley and Lewan, 2018; Schmidt et al., 2019).

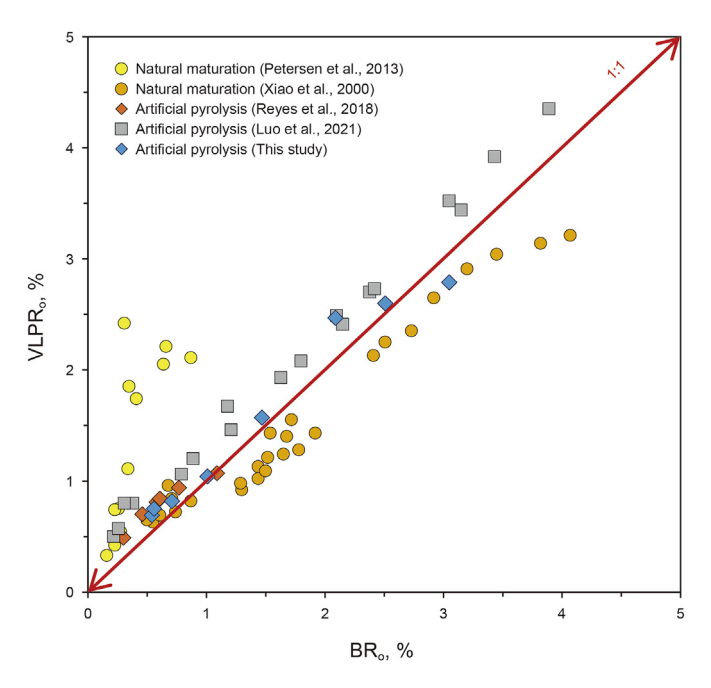


Fig. 19. Cross-plot comparing BR_o and $VLPR_o$ between naturally matured samples and artificially pyrolyzed residues.

low thermal maturities (Petersen et al., 2013). This potentially raises VLP's total aromaticity, hence elevating its relative reflectance. Even though the current study does not provide direct evidence concerning the impact of radioactive uranium on the

evolution of vitrinite-like material reflectance, it is highly likely that the organic material in the Alum shale appears to be slightly more stable than that of marine shales that are not as rich in uranium (Schulz et al., 2021). As a result, the reflectance of VLM in Alum shale, as an effective maturity proxy, may have a wider application range than the Lithuanian shale under study. We suggest that more studies would be useful to understand the details of the role radioactive uranium.

4.3. Vitrinite-like materials reflectance as a maturity proxy

Vitrinite-like materials have been a long-standing research topic. The reflectance of VLM or VLP has been proved to be a maturity evaluation indicator for Paleozoic and Precambrian source rocks (Buchardt and Lewan, 1990; Wang et al., 1996; Xiao et al., 2000; Petersen et al., 2013; Schmidt et al., 2015; Schito et al., 2017; Sorci et al., 2020; Luo et al., 2021). In the present study, the VLP exhibits distinct morphological and organic petrological features in comparison to SB. The VLP shaped lenses are discrete solitary particles and structureless in internal texture, oriented parallel to the plane (Fig. 4(i) and (k)). Some VLPs are filled with fine dispersed pyrite grains (Fig. 8(c)), exhibiting indigenous properties, while those with embedded framboidal pyrite show higher reflectance. The VLP is primarily non-fluorescent, with only a very small proportion exhibiting brown fluorescence (Fig. 4(j)). This may be due to changes in initial hydrogen content (Hartkopf-Fröder et al., 2015). It is also possible that some of the VLP may be subject to bacterial degradation and alteration, similar to bituminite (Synnott et al., 2016; Luo et al., 2021). In previous studies, Population H was regarded as a VLM, likely derived from a primitive plant source in Devonian shales (Araujo et al., 2014; Schmidt et al.,

 Table 4

 Characteristics of vitrinite-like materials in Precambrian-Paleozoic sediments.

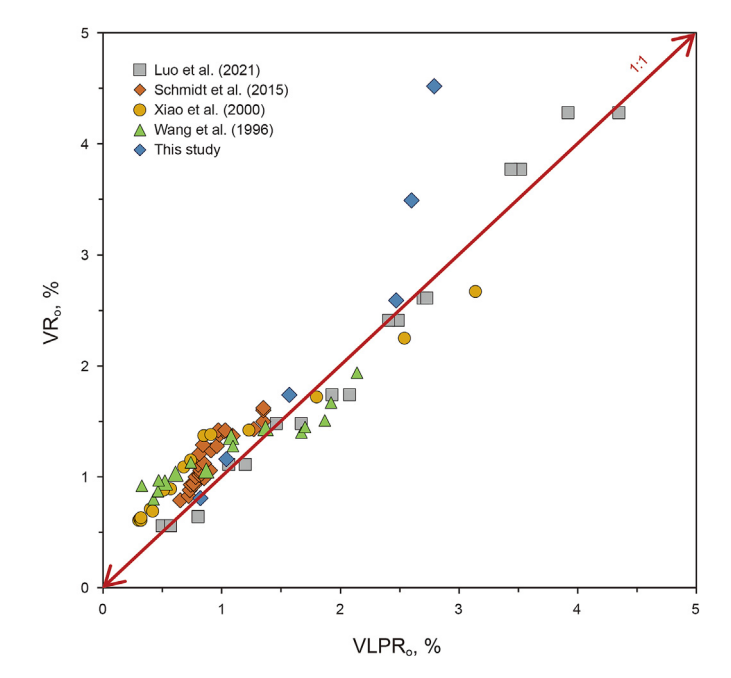
Sample, Region	Age	Morphology	Optical diagnos	tic characteristics		Origin	Publication
	_		Transmitted light	reflected light	Fluorescence properties		
Alum shale, Scandinavia	Middle Cambrian-Lower Ordovician	boundinage, lenticular, wavy, or tabular shapes; containing framboidal pyrite; size: $20-80~\mu m$ (lenths), $4-10~\mu m$ (widths)	Translucent yellowish orange (immature) Opaque black (post mature)	Gray to gray white	Lack of fluorescence	Gelification of polysaccharides diverse origins (multicellular algal seaweeds, fungal hyphae, and arthropod cuticle)	
Marine carbonate rocks, North China	Carboniferous		Orange yellow to orange red (early maturity); Orange red to brown (late maturity); Brown-black (over mature)	Blackish-brown to gray (early maturity); Gray to gray white (late maturity); White gray (over mature)	Orange yellow to orange red (early maturity); Orange red to brown (late maturity); Brown to non- fluorescence (over mature)	Humification of marine lower organism (algae, fungi)	Zhong and Qin (1995)
Oil shale (Kukersite), Estonia	Middle Ordovician	Sharp outline; spherical, block-like graininess and uniform internal texture; containing framboidal pyrite; size: $3{-}100~\mu m$	Brown, black brown	Gray white, white fine-medium grained mosaic texture (overmature)	Lack of fluorescence	Algae and their in situ degradation residual products	Wang et al. (1996)
Lower Paleozoic Tarim Basin, China	Lower Paleozoic	Lens-shaped, irregular strip shaped; elongate shape, homogenous texture and weak anisotropy; size: 5–15 μm	Reddish brown		Dark brown fluorescence	Origins from faunal organic matter, as a result of biochemical degradation by bacteria in a strongly reducing environment	Xiao et al. (1997)
Hydrocarbon source rocks, Tarim Basin, China	Lower Palaeozoic Carboniferous	Elongate, irregular lenticular, angular or rounded; homogenous texture; size: $20150~\mu\text{m}$, paralleling the bedding plane; Sometimes with pyrite grains smooth homogenous surface without internal structures	•	Dark gray to greyish white; weak anisotropy	Dark brown	Gelification of algal-derived organic matter	Xiao et al. (2000)
Ordovician and Silurian (Tanezzuft) source rock, Murzuq Basin, SW Libya	Lower Silurian Hot Shale, Tanezzuft and Ordovician	Sharp outlines, elongate fragments, angular shapes, and a smooth, structureless internal texture	1	Gray to gray white	Non- fluorescing	Unknown origin in a restricted distal marine environment	Belaid et al. (2010)
Alum shale, southern Scandinavia	Middle Cambrian-Lower Ordovician	Lenticular, wavy, or tabular shapes; some with a porous/granular surface	1	Dark gray to greyish white	Orange-brown fluorescence	Fragments of graptolites	Petersen et al. (2013)
Ponta Grossa Formation, Paraná basin	Devonian	Elongate, irregularly shaped; size: lens $20\!-\!150~\mu m$ long, paralleling the bedding plane	1	Dark gray to gray white	Dark brown fluorescence	Population H; A primitive plant source	Schmidt et al. (2015)
Eastern part of Moesian platform- Romanian sector	Devonian- Silurian	Homogeneous particles. Two main populations with different reflectance occur	1	1	1	The first population does not present any evidence of bitumen-related features and does not derived from graptolites; The second population may represent graptolite remains	Colțoi et al.

Boas River Formation Hudson Bay basin, Canada	Upper Ordovician Lı	Upper Ordovician Lenticular lens-shaped, elongated, rounded	/ Dark g white	ray to gray		Similar to bituminite, comprised of algal and Reyes et al. bacterial remains (2018)	Reyes et al. (2018)
Xiamaling shale, North China	Mesoproterozoic Lon μm	Xiamaling shale, $$ Mesoproterozoic $$ Long strip shape, similar to the morphology of bituminite size: tens of North China		o gray	Dark brown to non- fluorescing	Dark brown to Bacterial degradation (such as sulfate-reducing Luo et al. non-bacteria and methanogens) of lamalginite and/ (2021) fluorescing or bituminite under anoxic environments	ng Luo et al. d/ (2021)
Alum shale, Scandinavia	Middle Cambrian S _l	Middle Cambrian Spherical or oval in sections parallel to bedding, and elongate in sections perpendicular to bedding: lengths (20–150 µm) and widths (5–20 µm)		Dark gray	Lack of fluorescence	Might be akinete cells	Luo et al. (2021)
Wufeng- Longmaxi shales,	Upper Di Ordovician- si Lower Silurian ri	Dispersed OM particles with the shape being rounded or irregular. The size >5 μ m. Acritarchs occur as round OM particles with spikes on the rim, with a typical size of about 10–15 μ m	_	Gray white		Graptolite fragments; The round VLP are probably derived from acritarchs	Teng et al. (2022)
Baltic Basin, Lithuania	Upper Ordovician D	Upper Ordovician Discrete solitary particle; irregularly ellipsoidal or oval shape in sections perpendicular to bedding. Homogenous texture		Dark gray	Faint brown to non-luorescing	Faint brown to A fair amount of VLP does not consist of non-luorescing graptolite-type fragments. In-situ residue modures of alose degradation and alteration	This study

/: No description.

2015). It is an organic constituent that resembles vitrinite morphologically but has distinct chemistry and substantially lower reflectance than true vitrinite (Araujo et al., 2014). Until now, there are still different understandings of the origin for VLM or VLP. A number of published articles on the origins and characteristics of vitrinite-like materials have been summarized in Table 4. These analyses of the optical properties and thermal stress response to vitrinite-like materials are based on research on diverse marine shales around the world with varying geological ages, focusing solely on occurrence and optical characteristics. This seems to imply that the identified vitrinite-like materials, which are analyzed based on their appearance in various shale formations, may not be the same type.

Comparative analysis between this study and those by Luo et al. (2021), Schmidt et al. (2015), Xiao et al. (2000) and Wang et al. (1996) reveal similar overall result with respect to VLMR_o/VLPR_o and VR₀ correlation (Fig. 20). It was observed that the reflectance of VLP was clearly lower than that of vitrinite until VR₀ reached ≥1.5%–2.0%. The relationship for converting VLPR_o to EqVR_o from Carboniferous source rocks of Tarim Basin was divided into three stages, rather than a simple linear relation (Xiao et al., 2000). Schmidt et al. (2015) confirmed that the maturation pathway of the VLM is lower than that of vitrinite via hydrous pyrolysis based on Devonian marine shale. Luo et al. (2021) reported the VLM in Xiamaling shale disappeared after pyrolysis at 350 °C. Additionally, a marked discrepancy exists in Alum shale (Fig. 20). Initially, Buchardt and Lewan (1990) investigated VLM in the Alum shale response to thermal stress and discovered an inverse association between reflectance values and the atomic H/C ratios. Hackley and Lewan (2018) subsequently asserted that no VLM was identified in their Alum shale hydrous pyrolysis series. Contrary to the VLMR_o in the Cambrian Alum shale (Luo et al., 2021), which is constantly equivalent to the VR₀, a positive linear relation is present (Fig. 20). Our data trend is similar to that observed by Wang et al. (1996). The VLPR_o in Ordovician shales as an effective maturity proxy is less than 2.0% due to optical anisotropy development (Wang et al., 1996). This implies that VLP/VLM presented in shales with the same geologic time could have formed from the same starting



 $\textbf{Fig. 20.} \ \, \text{Cross-plot comparing VR}_o \ \, \text{and VLPR}_o \ \, \text{variations in laboratory-produced artificially matured residues.}$

materials and have similar thermal evolution behavior. To verify the hypothesis that their origins are influenced by original depositional environment or biodegradation, it is necessary to explore biochemistry characteristics. Further investigations are warranted on variations in the chemical structure evolution and hydrocarbon generation potential of VLP in shales of diverse geologic ages during thermal advance. In the meantime, a clear guideline and standard for vitrinite-like material and solid bitumen identification as well as maturity proxies need to reach a future consensus.

5. Conclusions

In this work, an Upper Ordovician zooclasts-bearing shale and a Middle Jurassic coal were compared via co-anhydrous pyrolysis to identify differences in the maturation pathways and morphology evolution between marine-derived DOM and terrigenous vitrinite. The following conclusions can be drawn:

The marine-derived DOM components in this sample are composed of solid bitumen, bituminite, chitinozoans, a few graptolites, VLP, residual Tasmanite and liptodetrinite. The reflectance sequence from high to low is zooclasts, VLP and SB. Their reflectances gradually increase as the pyrolysis temperature rises, although the rate of growth is slower than that of co-heating coal vitrinite.

Zooclasts yield significantly higher reflectance values than the VLP and SB at each pyrolysis temperature. Chitinozoans and graptolites have comparable average reflectance values. Laboratory simulated maturation results demonstrate that zooclasts have the same thermal stress as vitrinite, and the reflectance of graptolites and chitinozoans has the same growth rate. Reflectance correlations among the DOM were established. The VLPR₀, an OM maturity evaluation proxy, is applicable to reflectance values less than 2.0% in Ordovician shales, unlike VLM in Cambrian Alum shales. The vitrinite-like materials in the Paleozoic sediments from various geological periods seem to have a diverse of origins and multiple evolution pathways as thermal maturity increases.

Consideration of measurement directionality is crucial when we apply reflectance studies and interpret reflectance values of Lower Paleozoic sediments. This investigation enhanced understandings of marine-derived DOM evolution issues, providing clearer correlations among reflectances of different DOM and reducing uncertainties in thermal maturity determination.

CRediT authorship contribution statement

Ye Wang: Writing — review & editing, Writing — original draft, Methodology, Investigation, Funding acquisition, Data curation, Conceptualization. **Zhong-Liang Ma:** Visualization, Investigation, Funding acquisition. **Nan-Sheng Qiu:** Writing — review & editing, Project administration, Funding acquisition, Conceptualization. **Bao-Jian Shen:** Resources. **Xiao-Min Xie:** Supervision, Methodology, **Tenger Borjigin:** Resources. **Lun-Ju Zheng:** Methodology, Investigation. **Zhao-Xi Zuo:** Formal analysis. **An-Yang Pan:** Resources.

Funding information

National Natural Science Foundation of China (No. 42202172; U24B6001; No. 41830424). The Fundamental Research Funds for the Central Universities, CHD (300102274202).

Declaration of competing interest

The authors declare that they have no known competing financial interests or personal relationships that could have appeared to influence the work reported in this paper.

Acknowledgements

This paper was supported by National Natural Science Foundation of China (Nos. 42202172, U24B6001, 41830424) and the Fundamental Research Funds for the Central Universities, CHD (300102274202). The authors would like to express their appreciation to Prof. Amalia Spina and three anonymous reviewers for their detailed and constructive reviews. Dr. Bin Wu is thanked for English proofreading and polishing.

References

- Araujo, C.V., Borrego, A.G., Cardott, B., Chagas, R.B.A., Flores, D., Gonçalves, P., Hackley, P.C., Hower, J.C., Kern, M.L., Kus, J., Mastalerz, M., Filho, J.G.M., Mendonça, J.O., Menezes, T.R., Newman, J., Suarez-Ruiz, I., Silva, F.S., Souza, I.V.A.F., 2014. Petrographic maturity parameters of a devonian shale maturation series, appalachian basin, USA. ICCP thermal indices working group interlaboratory exercise. Int. J. Coal Geol. 130, 89–101. https://doi.org/10.1016/i.coal.2014.05.002.
- ASTM, 2015. D7708 standard test method for microscopical determination of the reflectance of vitrinite dispersed in sedimentary rocks, petroleum products, lubricants, and fossil fuels. Gaseous Fuels; Coal and Coke, Sec. V. 05.06. ASTM International, West Conshohocken, PA 5. https://doi.org/10.1520/D7708-14.
- Behar, F., Lewan, M.D., Lorant, F., Vandenbroucke, M., 2003. Comparison of artificial maturation of lignite in hydrous and nonhydrous conditions. Org. Geochem. 34, 575–600. https://doi.org/10.1016/S0146-6380(02)00241-3.
- Belaid, A., Krooss, B.M., Littke, R., 2010. Thermal history and source rock characterization of a paleozoic section in the awbari trough, murzuq basin, SW Libya. Mar. Petrol. Geol. 27 (3), 612–632. https://doi.org/10.1016/j.marpetgeo.2009.06.006.
- Berg, R.R., Gangi, A.F., 1999. Primary migration by oil-generation microfracturing in low-permeability source rocks: application to the austin chalk, Texas. AAPG (Am. Assoc. Pet. Geol.) Bull. 83, 727–756. https://doi.org/10.1306/E4FD2D6B-1732-11D7-8645000102C1865D.
- Bertrand, R., 1990. Correlations among the reflectances of vitrinite, chitinozoans, graptolites and scolecodonts. Org. Geochem. 15 (6), 565–574. https://doi.org/10.1016/0146-6380(90)90102-6.
- Bertrand, R., Lavoie, D., Fowler, M., 2003. Cambrian—Ordovician shales in the Humber Zone: thermal maturation and source rock potential. Bull. Can. Petrol. Geol. 51, 213—233. https://doi.org/10.2113/51.3.213.
- Bertrand, R., Malo, M., 2001. Source rock analysis, thermal maturation and hydrocarbon generation in the Siluro-Devonian rocks of the Gaspé Belt Basin. Bull. Can. Petrol. Geol. 49, 238–261. https://doi.org/10.2113/49.2.238.
- Bertrand, R., Malo, M., 2012. Dispersed Organic Matter Reflectance and Thermal Maturation in Four Hydrocarbon Exploration Wells in the Hudson Bay Basin: Regional Implications. Geol. Surv. Canada, pp. 1–52. https://doi.org/10.4095/289709.
- Bertrand, R., Yvon Héroux, Y., 1987. Chitinozoan, graptolite, and scolecodont reflectance as an alternative to vitrinite and pyrobitumen reflectance in Ordovician and Silurian strata, Anticosti Island, Quebec, Canada. AAPG (Am. Assoc. Pet. Geol.) Bull. 71 (8), 951–957. https://doi.org/10.1029/JB092iB09p09452.
- Buchardt, B., Lewan, M.D., 1990. Reflectance of vitrinite-like macerals as a thermal maturity index for Cambrian-Ordovician Alum shale, southern Scandinavia. AAPG (Am. Assoc. Pet. Geol.) Bull. 74, 394–406. https://doi.org/10.1029/ JB095iB04p05171.
- Buratti, N., De Luca, R., Garuti, L., Sorci, A., Spina, A., Clayton, G., 2024. Thermal maturity evaluation on mildly artificially oxidised sporomorphs: a comprehensive calibration of palynomorph darkness index (PDI) with vitrinite reflectance. Mar. Petrol. Geol. 162, 106672. https://doi.org/10.1016/ i.marpetgeo.2023.106672.
- Bustin, R.M., Link, C., Goodarzi, F., 1989. Optical properties and chemistry of graptolite periderm following laboratory simulated maturation. Org. Geochem. 14, 355–364. https://doi.org/10.1016/0146-6380(89)90001-6.
- Caricchi, C., Sveva Corrado, S., Paolo, L.D., Luca Aldega, L., Grigo, D., 2016. Thermal maturity of silurian deposits in the baltic syneclise (on-shore polish Baltic Basin): contribution to unconventional resources assessment. Italian Journal of Geosciences 135 (3), 383–393. https://doi.org/10.3301/IJG.2015.16.
- Carr, A.D., 2000. Suppression and retardation of vitrinite reflectance, part 1: formation and significance for hydrocarbon generation. J. Petrol. Geol. 23, 313—343. https://doi.org/10.1111/j.1747-5457.2000.tb01022.x.
- Carvajal-Ortiz, H., Gentzis, T., 2015. Critical considerations when assessing hydrocarbon plays using Rock-Eval pyrolysis and organic petrology data: data quality revisited. Int. J. Coal Geol. 152, 113—122. https://doi.org/10.1016/ j.coal.2015.06.001.
- Cavelan, A., Boussafir, M., Le Milbeau, C., Rozenbaum, O., Laggoun-Défarge, F., 2019. Effect of organic matter composition on source rock porosity during confined anhydrous thermal maturation: example of Kimmeridge-clay mudstones. Int. J. Coal Geol. 212, 103236. https://doi.org/10.1016/j.coal.2019.103236.
- Cichon-Pupienis, A., Littke, R., Froidl, F., Lazauskiene, J., 2020. Depositional history, source rock quality and thermal maturity of Upper Ordovician lower Silurian organic-rich sedimentary rocks in the central part of the Baltic Basin

(Lithuania). Mar. Petrol. Geol. 112, 104083. https://doi.org/10.1016/j.marpetgeo.2019.104083.

- Cichon-Pupienis, A., Littke, R., Lazauskiene, J., Baniasad, A., Pupienis, D., Radzevicius, S., Siliauskas, L., 2021. Geochemical and sedimentary facies study; implication for driving mechanisms of organic matter enrichment in the lower Silurian fine-grained mudstones in the Baltic Basin (W Lithuania). Int. J. Coal Geol. 244, 103815. https://doi.org/10.1016/j.coal.2021.103815.
- Cole, G.A., 1994. Graptolite—chitinozoan reflectance and its relationship to other geochemical maturity indicators in the Silurian Qusaiba Shale, Saudi Arabia. Energy & Fuels 8, 1443—1459. https://doi.org/10.1021/ef00048a035.
- Coltoi, O., Nicolas, G., Safa, P., 2016. The assessment of the hydrocarbon potential and maturity of Silurian intervals from eastern part of Moesian Platform Romanian sector. Mar. Petrol. Geol. 77, 653—667. https://doi.org/10.1016/j.marpetgeo.2016.06.024.
- Dahl, J., Hallberg, R., Kaplan, I., 1988. Effects of irradiation from uranium decay on extractable organic matter in the Alum Shales of Sweden. Org. Geochem. 12, 559–571. https://doi.org/10.1016/0146-6380(88)90147-7.
- Espitalié, J., Deroo, G., Marquis, F., 1985. La pyrolyse Rock-Eval et ses applications. Première partie. Oil & Gas Science and Technology-revue De L Institut Francais Du Petrole 40, 563–579. https://doi.org/10.2516/ogst:1985035.
- Fishman, N.S., Hackley, P.C., Lowers, H.A., Hill, R.J., Egenhoff, S.O., Eberl, D.D., Blum, A.E., 2012. The nature of porosity in organic-rich mudstones of the upper jurassic kimmeridge clay formation, North sea, offshore United Kingdom. Int. J. Coal Geol. 103, 32–50. https://doi.org/10.1016/j.coal.2012.07.012.
- Gentzis, T., Freitas, T., Goodarzi, F., Melchin, M., Lenz, A., 1996. Thermal maturity of lower paleozoic sedimentary successions in arctic Canada. AAPG (Am. Assoc. Pet. Geol.) Bull. 80, 1065–1084. https://doi.org/10.1306/64ED8C96-1724-11D7-8645000102C1865D.
- Glikson, M., Taylor, D., Morris, D., 1992. Lower Palaeozoic and Precambrian petroleum source rocks and the coalification path of alginite. Org. Geochem. 18, 881–897. https://doi.org/10.1016/0146-6380(92)90056-4.
- Gonçalves, P.A., Kus, J., Hackley, P.C., Borrego, A.G., Hámor-Vidó, M., Kalkreuth, W., Mendonça Filho, J.G., Petersen, H.I., Pickel, W., Reinhardt, M.J., Suárez-Ruiz, I., 2024. The petrology of dispersed organic matter in sedimentary rocks: review and update. Int. J. Coal Geol. 294, 104604. https://doi.org/10.1016/i.coal.2024.104604.
- Goodarzi, F., Fowler, M., Bustin, M., McKirdy, D., 1992. Thermal maturity of early paleozoic sediments. As determined by the optical properties of marine-derived organic matter—a review, early organic evolution. Implications for Mineral and Energy Resources. Springer, pp. 279–295. https://doi.org/10.1007/978-3-642-76884-2-21
- Goodarzi, F., Norford, B., 1987. Optical properties of graptolite epiderm—a review. Bulletin of Geology Society Denmark 35, 141–147. https://doi.org/10.37570/bgsd-1986-35-15.
- Goodarzi, F., Norford, B., 1989. Variation of graptolite reflectance with depth of burial. Int. J. Coal Geol. 11, 127–141. https://doi.org/10.1016/0166-5162(89) 90002-5.
- Goodarzi, F., Snowdon, L., Gunther, P., Jenkins, W., 1985. Preliminary organic petrography of palaeozoic rocks from the grand banks, newfoundland. Mar. Petrol. Geol. 2, 254–259. https://doi.org/10.1016/0264-8172(85)90015-7.
- Hackley, P.C., Araujo, C.V., Borrego, A.G., Bouzinos, A., Cardott, B., Cook, A.C., Eble, C., Flores, D., Gentzis, T., Gonçalves, P.A., Mendonça Filho, J.G., Hámor-Vidó, M., Jelonek, I., Kommeren, K., Knowles, W., Kus, J., Mastalerz, M., Menezes, T.R., Newman, J., Oikonomopoulos, I.K., Pawlewicz, M., Pickel, W., Potter, J., Ranasinghe, P., Read, H., Reyes, J., Rodriguez, G.D.L.R., Fernandes de Souza, I.V.A., Suarez-Ruiz, I., Sýkorová, I., Valentine, B.J., 2015. Standardization of reflectance measurements in dispersed organic matter: results of an exercise to improve interlaboratory agreement. Mar. Petrol. Geol. 59, 22–34. https://doi.org/10.1016/j.marpetgeo.2014.07.015.
- Hackley, P.C., Cardott, B.J., 2016. Application of organic petrography in North American shale petroleum systems: a review. Int. J. Coal Geol. 163, 8–51. https://doi.org/10.1016/j.coal.2016.06.010.
- Hackley, P.C., Jubb, A.M., Smith, P.L., Mcaleer, R.J., Valentine, B.J., Hatcherian, J., Botterell, P.J., Birdwell, J.E., 2022. Evaluating aromatization of solid bitumen generated in the presence and absence of water: implications for solid bitumen reflectance as a thermal proxy. Int. J. Coal Geol. 258, 104016. https://doi.org/10.1016/j.coal.2022.104016.
- Hackley, P.C., Lewan, M., 2018. Understanding and distinguishing reflectance measurements of solid bitumen and vitrinite using hydrous pyrolysis: implications to petroleum assessment. AAPG (Am. Assoc. Pet. Geol.) Bull. 102, 1119–1140. https://doi.org/10.1306/08291717097.
- Hackley, P.C., Valentine, B.J., Hatcherian, J.J., 2018. On the petrographic distinction of bituminite from solid bitumen in immature to early mature source rocks. Int. J. Coal Geol. 196, 232–245. https://doi.org/10.1016/j.coal.2018.06.004.
- Haeri-Ardakani, O., Sanei, H., Lavoie, D., Chen, Z., Jiang, C., 2015. Geochemical and petrographic characterization of the upper ordovician utica shale, southern quebec, Canada. Int. J. Coal Geol. 138, 83–94. https://doi.org/10.1016/ i.coal.2014.12.006.
- Harkopf-Fröder, C., Königshof, P., Littke, R., Schwarzbauer, J., 2015. Optical thermal maturity parameters and organic geochemical alteration at low grade diagenesis to anchimetamorphism: a review. Int. J. Coal Geol. 163, 8–51. https:// doi.org/10.1016/j.coal.2015.06.005.
- Jarvie, D.M., Claxton, B., Henk, B., Breyer, J., 2001. Oil and shale gas from the barnett shale, Ft.Worth basin, Texas. In: AAPG National Convention. Denver, CO, USA

- June 3–6 (AAPG Search and Discovery Article #90906). http://www.searchanddiscovery.com/abstracts/html/2001/annual/abstracts/0386.htm.
- Klaja, J., Przelaskowska, A., Kulinowski, P., Bujok, P., Klempa, M., 2020. Investigation of fine-grained siliciclastic rocks of different clay content using thermal methods. J. Petrol. Sci. Eng. 184, 106531. https://doi.org/10.1016/ j.petrol.2019.106531.
- Ko, L.T., Loucks, R.G., Zhang, T., Ruppel, S.C., Shao, D., 2016. Pore and pore network evolution of Upper Cretaceous Boquillas (Eagle Ford—equivalent) mudrocks: results from gold tube pyrolysis experiments. AAPG (Am. Assoc. Pet. Geol.) Bull. 100, 1693—1722. https://doi.org/10.1306/04151615092.
- Ko, L.T., Ruppel, S.C., Loucks, R.G., Hackley, P.C., Zhang, T., Shao, D., 2018. Pore-types and pore-network evolution in Upper Devonian-Lower Mississippian Woodford and Mississippian Barnett mudstones: insights from laboratory thermal maturation and organic petrology. Int. J. Coal Geol. 190, 3–28. https://doi.org/ 10.1016/j.coal.2017.10.001.
- Kotarba, M.J., Lewan, M.D., 2013. Sources of natural gases in Middle Cambrian reservoirs in Polish and Lithuanian Baltic Basin as determined by stable isotopes and hydrous pyrolysis of Lower Palaeozoic source rocks. Chem. Geol. 345, 62–76. https://doi.org/10.1016/j.chemgeo.2013.02.023.
- Lavoie, D., Pinet, N., Bordeleau, G., Ardakani, O.H., Ladevèze, P., Duchesne, M.J., Rivard, C., Mort, A., Brake, V., Sanei, H., Malet, X., 2016. The Upper Ordovician black shales of southern Quebec (Canada) and their significance for naturally occurring hydrocarbons in shallow groundwater. Int. J. Coal Geol. 158, 44–64. https://doi.org/10.1016/j.coal.2016.02.008.
- Liu, B., Mastalerz, M., Schieber, J., 2022. SEM petrography of dispersed organic matter in black shales: a review. Earth Sci. Rev. 224, 103874. https://doi.org/ 10.1016/j.earscirev.2021.103874.
- Liu, B., Schieber, J., Mastalerz, M., 2017. Combined SEM and reflected light petrography of organic matter in the New Albany Shale (Devonian-Mississippian) in the Illinois Basin: a perspective on organic pore development with thermal maturation. Int. J. Coal Geol. 184, 57–72. https://doi.org/10.1016/j.coal.2017.11.002.
- Luo, Q., Zhang, L., Zhong, N., Wu, J., Goodarzi, F., Sanei, H., Skovsted, C.B., Suchý, V., Li, M., Ye, X., Gao, W., Liu, A., Min, X., Pan, Y., Yao, L., Wu, J., 2021. Thermal evolution behavior of the organic matter and a ray of light on the origin of vitrinite-like maceral in the Mesoproterozoic and Lower Cambrian black shales: insights from artificial maturation. Int. J. Coal Geol. 244, 103813. https://doi.org/10.1016/j.coal.2021.103813.
- Luo, Q., Fariborz, G., Zhong, N., Wang, Y., Qiu, N., Skovsted, C.B., Suchý, V., Schovsbo, N.H., Morga, R., Xu, Y., Hao, J., Liu, A., Wu, J., Cao, W., Min, X., Wu, J., 2020. Graptolites as fossil geo-thermometers and source material of hydrocarbons: an overview of four decades of progress. Earth Sci. Rev. 200, 103000. https://doi.org/10.1016/j.earscirev.2019.103000.
- Luo, Q., Goodarzi, F., Zhong, N., Qiu, N., Wang, X., Suchý, V., Khan, I., Zheng, X., Liu, B., Ardakani, O.H., Zhang, Y., Li, D., Wu, J., Fang, Z., Shi, R., Skovsted, C.B., Sanei, H., Xu, Y., Hu, W., Duan, G., 2025. Dispersed organic matter from pre-Devonian marine shales: a review on its composition, origin, evolution, and potential for hydrocarbon prospecting. Earth Sci. Rev. 261, 105027. https://doi.org/10.1016/j.earscirev.2024.105027.
- Luo, Q., Hao, J., Skovested, C.B., Xu, Y., Liu, Y., Wu, J., Zhang, S., Wang, W., 2018. Optical characteristics of graptolite-bearing sediments and its implication for thermal maturity assessment. Int. J. Coal Geol. 195, 386–401. https://doi.org/ 10.1016/j.coal.2018.06.019.
- Malinconico, M.A.L., 1993. Reflectance cross-plot analysis of graptolites from the anchimetamorphic region of northern Maine. USA Organic Geochemistry 20, 197–207. https://doi.org/10.1016/0146-6380(93)90038-D.
- Mastalerz, M., Drobniak, A., Stankiewicz, A.B., 2018. Origin, properties, and implications of solid bitumen in source-rock reservoirs: a review. Int. J. Coal Geol. 195, 14–36. https://doi.org/10.1016/j.coal.2018.05.013.
- Mählmann, F.R., Bayon, R.L., 2016. Vitrinite and vitrinite like solid bitumen reflectance in thermal maturity studies: correlations from diagenesis to incipient metamorphism in different geodynamic settings. Int. J. Coal Geol. 157, 52–73. https://doi.org/10.1016/j.coal.2015.12.008.
- Mishra, D.K., Hackley, P.C., Jubb, A.M., Sanders, M.M., Agrawal, S., Varma, A.K., 2022. Maturation study of vitrinite in carbonaceous shales and coals: insights from hydrous pyrolysis. Int. J. Coal Geol. 259, 104044. https://doi.org/10.1016/ j.coal.2022.104044.
- Obermajer, M., Fowler, M.G., Goodarzi, F., Snowdon, L.R., 1996. Assessing thermal maturity of Palaeozoic rocks from reflectance of chitinozoa as constrained by geochemical indicators: an example from southern Ontario, Canada. Mar. Petrol. Geol. 13 (8), 907–919. https://doi.org/10.1016/S0264-8172(96)00036-0.
- Paškevičius, J., 1997. The Geology of the Baltic Republics. Lietuvos geologijos tarnyba, Vilnius. http://www.digar.ee/id/nlib-digar:651201. ISBN 9789916069059.
- Peters, K., Hackley, P., Thomas, J. Pomerantz A., 2018. Suppression of vitrinite reflectance by bitumen generated from liptinite during hydrous pyrolysis of artificial source rock. Org. Geochem. 125, 220–228. https://doi.org/10.1016/ J.ORGGEOCHEM.2018.09.010.
- Petersen, H.I., Schovsbo, N.H., Nielsen, A.T., 2013. Reflectance measurements of zooclasts and solid bitumen in Lower Paleozoic shales, southern Scandinavia: correlation to vitrinite reflectance. Int. J. Coal Geol. 114, 1–18. https://doi.org/ 10.1016/j.coal.2013.03.013.
- Reyes, J., Jiang, C., Lavoie, D., Armstrong, D.K., Milovic, M., Robinson, R., 2018. Organic petrographic analysis of artificially matured chitinozoan- and graptolite-rich Upper Ordovician shale from Hudson Bay Basin, Canada. Int. J. Coal Geol. 199, 138–151. https://doi.org/10.1016/j.coal.2018.09.019.

Riediger, C., Goodarzi, F., Macqueen, R.W., 1989. Graptolites as indicators of regional maturity in lower Paleozoic sediments, Selwyn Basin, Yukon and northwest Territories, Canadian. J. Earth Sci. 26, 2003–2015. https://doi.org/10.1139/e89-169

- Schito, A., Corrado, S., Trolese, M., Aldega, L., Caricchi, C., Cirilli, S., Grigo, D., Guedes, A., Romano, C., Spina, A., Valentim, B., 2017. Assessment of thermal evolution of paleozoic successions of the holy cross mountains (Poland). Mar. Petrol. Geol. 80, 112–132. https://doi.org/10.1016/j.marpetgeo.2016.11.016.
- Schito, A., Spina, A., Corrado, S., Cirilli, S., Romano, C., 2019. Comparing optical and Raman spectroscopic investigations of phytoclasts and sporomorphs for thermal maturity assessment: the case study of Hettangian continental facies in the Holy cross Mts. (central Poland). Mar. Petrol. Geol. 104, 331–345. https:// doi.org/10.1016/j.marpetgeo.2019.03.008.
- Schmidt, J.S., Araujö, C.V., Souza, I.V., Chagas, R.B., 2015. Hydrous pyrolysis maturation of vitrinite-like and humic vitrinite macerals: implications for thermal maturity analysis. Int. J. Coal Geol. 144, 5–14. https://doi.org/10.1016/i.coal.2015.03.016.
- Schmidt, J.S., Menezes, T.R., Souza, I.V.A.F., Spigolon, A.L.D., Pestilho, A.L.S., Coutinho, L.F.C., 2019. Comments on empirical conversion of solid bitumen reflectance for thermal maturity evaluation. Int. J. Coal Geol. 201, 44–50. https://doi.org/10.1016/j.coal.2018.11.012.
- Schoenherr, J., Littke, R., Urai, J.L., Kukla, P.A., Rawahi, Z., 2007. Polyphase thermal evolution in the Infra-Cambrian Ara Group (South Oman Salt Basin) as deduced by maturity of solid reservoir bitumen. Org. Geochem. 38, 1293—1318. https://doi.org/10.1016/j.orggeochem.2007.03.010.
- Schulz, H., Yang, S., Schovsbo, N.H., Rybacki, E., Ghanizadeh, A., Bernard, S., Mahlstedt, N., Krüger, M., Amann-Hildebrandt, A., Krooss, B.M., Meieri, T., Reinicke, A., 2021. The furongian to lower ordovician alum shale formation in conventional and unconventional petroleum systems in the Baltic Basin a review. Earth Sci. Rev. 218, 103674. https://doi.org/10.1016/j.earscirev.2021.103674.
- Song, J., Hackley, P.C., Sanders, M.M., Jubb, A.M., Luo, Q., 2023. Thermal evolution of graptolite and solid bitumen properties at high maturity under natural and artificial conditions. Int. J. Coal Geol. 273, 104269. https://doi.org/10.1016/ i.coal.2023.104269.
- Sorci, A., Cirilli, S., Clayton, G., Corrado, S., Hints, O., Goodhue, R., Schito, A., Spina, A., 2020. Palynomorph optical analyses for thermal maturity assessment of Upper Ordovician (Katian-Hirnantian) rocks from Southern Estonia. Mar. Petrol. Geol. 120, 1–15. https://doi.org/10.1016/j.marpetgeo.2020.104574.
- Spina, A., Cirilli, S., Sorci, A., Schito, A., Clayton, G., Corrado, S., Fernandes, P., Galasso, F., Montesi, G., Pereira, Z., Rashidi, M., Rettori, R., 2021. Assessing thermal maturity through a multi-proxy approach: a case study from the permian faraghan formation (zagros basin, southwest Iran). Geosciences 11 (12), 484. https://doi.org/10.3390/geosciences11120484.
- Spina, A., Vecoli, M., Riboulleau, A., Clayton, G., Cirilli, S., Di Michele, A., Marcogiuseppe, A., Rettori, R., Sassi, P., Servais, T., Riquier, L., 2018. Application of Palynomorph Darkness Index (PDI) to assess the thermal maturity of palynomorphs: a case study from North Africa. Int. J. Coal Geol. 188, 64–78. https://doi.org/10.1016/j.marpetgeo.2020.10457.
- Suárez-Ruiz, I., Flores, D., Filho, J.G.M., Hackley, P.C., 2012. Review and update of the applications of organic petrology: part 1, geological applications. Int. J. Coal Geol. 99, 54–112. https://doi.org/10.1016/j.coal.2012.03.005.
- Synnott, D.P., Dewing, K., Ardakani, O.H., Obermajer, M., 2018. Correlation of zooclast reflectance with rock-eval Tmax values within upper ordovician cape phillips formation, a potential petroleum source rock from the Canadian Arctic Islands. Fuel 227, 165–176. https://doi.org/10.1016/j.fuel.2018.04.096.
- Synnott, D.P., Sanei, H., Pedersen, P.K., Dewing, K., Haeri-Ardakani, O., 2016. The effect of bacterial degradation on bituminite reflectance. Int. J. Coal Geol. 162, 34–38. https://doi.org/10.1016/j.coal.2016.05.016.
- Teng, J., Liu, B., Mastalerz, M., Schieber, J., 2022. Origin of organic matter and organic pores in the overmature Ordovician-Silurian Wufeng-Longmaxi shale of the

- Sichuan Basin, China. Int. J. Coal Geol. 253, 103970. https://doi.org/10.1016/j.coal.2022.103970.
- Tricker, P.M., Marshall, J., Badman, T.D., 1992. Chitinozoan reflectance: a Lower Palaeozoic thermal maturity indicator. Mar. Petrol. Geol. 9 (3), 302–307. https://doi.org/10.1016/0264-8172(92)90078-S.
- Vecoli, M., Delabroye, A., Spina, A., Hints, O., 2011. Cryptospore assemblages from upper Ordovician (Katian—Hirnantian) strata of Anticosti Island, Québec, Canada, and Estonia: palaeophytogeographic and palaeoclimatic implications. Rev. Palaeobot. Palynol. 166 (1–2), 76–93. https://doi.org/10.1016/j.revpalbo.2011.05.006.
- Wang, Y., Qiu, N., Tao, N., Xie, X., Zuo, Z., Ma, Z., Shen, B., Tenger, B., 2023. Thermal maturity calibration of extremely high-mature pre-Devonian strata: a case study from the Lower Cambrian Qiongzhusi Formation in the Sichuan Basin, South China. Geoenergy Science and Engineering 222, 211411. https://doi.org/ 10.1016/j.geoen.2022.211411.
- Wang, F., He, P., Cheng, D., Hao, S., Liu, D., 1996. The reflectance of vitrinite-like maceral can be used as the maturity indicator of the lower Palaeozoic highpostmature hydrocarbon source rocks. Nat. Gas. Ind. 4, 24–28 (in Chinese). https://doi.org/CNKI:SUN:TRQG.0.1996-04-003.
- Wang, Y., Qiu, N., Borjigin, T., Shen, B., Xie, X., Ma, Z., Lu, C., Yang, Y., Yang, L., Cheng, L., Fang, G., Cui, Y., 2019. Integrated assessment of thermal maturity of the Upper ordovician—lower silurian Wufeng—Longmaxi shale in Sichuan basin, China. Mar. Petrol. Geol. 100, 447–465. https://doi.org/10.1016/j.marpetgeo.2018.10.025.
- Wang, Y., Qiu, N., Ma, Z., Ning, C., Zheng, L., Zhou, Y., Fang, G., Rui, X., Rao, D., 2020. Evaluation of equivalent relationship between vitrinite reflectance and solid bitumen reflectance. J. China Inst. Min. Technol. 49 (3), 510–522. https:// doi.org/10.13247/j.cnki.jcumt.001114 (in Chinese).
- Wang, Y., Qiu, N., Xie, X., Ma, Z., Li, L., Feng, Q., Yang, L., Shen, B., Borjigin, T., Tao, N., 2021. Maturity and thermal evolution differences between two sets of Lower Palaeozoic shales and its significance for shale gas formation in south-western Sichuan Basin, China. Geol. J. 56, 3698–3719. https://doi.org/10.1002/gj.4121.
- Xiao, X., Liu, D., Fu, J., Wilkins, R., 1997. Marine vitrinite—an important hydrocarbon source matter in marine source rocks. Acta Petrol. Sin. 18 (1), 44–48. https://doi.org/10.7623/syxb199701008 (in Chinese).
- Xiao, X., Wilkins, R., Liu, D., Liu, Z., Fu, J., 2000. Investigation of thermal maturity of lower Palaeozoic hydrocarbon source rocks by means of vitrinite-like maceral reflectance—a Tarim Basin case study. Org. Geochem. 31, 1041–1052. https:// doi.org/10.1016/S0146-6380(00)00061-9.
- Yang, C., Hesse, R., 1993. Diagenesis and anchimetamorphism in an overthrust belt, external domain of the Taconian Orogen, southern Canadian Applachians—II. Paleogeothermal gradients derived from maturation of different types of organic matter. Org. Geochem. 20, 381–403. https://doi.org/10.1016/0146-6380(93)90127-W.
- Yang, S., Schulz, H.-M., Schovsbo, N.H., Wirth, R., Mayanna, S., 2019. The organic geochemistry of "Kolm," a unique analogue for the understanding of molecular changes after significant uranium irradiation. Int. J. Coal Geol. 209, 89–93. https://doi.org/10.1016/j.coal.2019.05.004.
- Zdanavičiūtė, O., Lazauskienė, J., 2009. Organic matter of Early Silurian succession the potential source of unconventional gas in the Baltic Basin (Lithuania). Baltica 22 (2), 89–99.
- Zheng, X., Sanei, H., Schovsbo, N.H., Luo, Q., Wu, J., Zhong, N., Galloway, G.M., Goodarzi, F., 2021. Role of zooclasts in the kerogen type and hydrocarbon potential of the lower Paleozoic alum shale. Int. J. Coal Geol. 248, 103865. https://doi.org/10.1016/j.coal.2021.103865.
- Zheng, X., Schovsbo, N.H., Luo, Q., Wu, J., Zhong, N., Goodarzi, F., Sanei, H., 2022. Graptolite reflectance anomaly. Int. J. Coal Geol. 261, 104072. https://doi.org/10.1016/j.coal.2022.104072.
- Zhong, N., Qin, Y., 1995. Organic Petrology of Carbonate Rocks: Characteristics, Origin and Evolution of Macerals with Respects to Hydrocarbon Generation. Science Press, Beijing (in Chinese). ISBN:9787030046505.